



Dynamics and stability of a power-law film flowing down a slippery slope

Cite as: Phys. Fluids **31**, 013102 (2019); <https://doi.org/10.1063/1.5078450>

Submitted: 25 October 2018 . Accepted: 14 December 2018 . Published Online: 08 January 2019

Symphony Chakraborty , Tony Wen-Hann Sheu, and Sukhendu Ghosh 



View Online



Export Citation



CrossMark

ARTICLES YOU MAY BE INTERESTED IN

[Capillary surface wave formation and mixing of miscible liquids during droplet impact onto a liquid film](#)

Physics of Fluids **31**, 012107 (2019); <https://doi.org/10.1063/1.5064640>

[Instabilities in viscosity-stratified two-fluid channel flow over an anisotropic-inhomogeneous porous bottom](#)

Physics of Fluids **31**, 012103 (2019); <https://doi.org/10.1063/1.5065780>

[Coalescence dynamics of unequal sized drops](#)

Physics of Fluids **31**, 012105 (2019); <https://doi.org/10.1063/1.5064516>

AIP Conference Proceedings
FLASH WINTER SALE!

50% OFF ALL PRINT PROCEEDINGS

ENTER CODE 50DEC19 AT CHECKOUT

Dynamics and stability of a power-law film flowing down a slippery slope

Cite as: Phys. Fluids 31, 013102 (2019); doi: 10.1063/1.5078450

Submitted: 25 October 2018 • Accepted: 14 December 2018 •

Published Online: 8 January 2019



View Online



Export Citation



CrossMark

Symphony Chakraborty,¹ Tony Wen-Hann Sheu,^{1,2} and Sukhendu Ghosh^{3,a)}

AFFILIATIONS

¹Center for Advanced Study in Theoretical Sciences, National Taiwan University, No. 1, Sec. 4, Roosevelt Road, Taipei 10617, Taiwan

²Department of Engineering Science and Ocean Engineering, National Taiwan University, No. 1, Sec. 4, Roosevelt Road, Taipei 10617, Taiwan

³Department of Mathematics, Presidency University, Kolkata 700073, India

^{a)}Author to whom correspondence should be addressed: sukhendu.math@gmail.com

ABSTRACT

A power-law fluid flowing down a slippery inclined plane under the action of gravity is deliberated in this research work. A Newtonian layer at a small strain rate is introduced to take care of the divergence of the viscosity at a zero strain rate. A low-dimensional two-equation model is formulated using a weighted-residual approach in terms of two coupled evolution equations for the film thickness h and a local velocity amplitude or the flow rate q within the framework of lubrication theory. Moreover, a long-wave instability is shown in detail. Linear stability analysis of the proposed two-equation model reveals good agreement with the spatial Orr-Sommerfeld analysis. The influence of a wall-slip on the primary instability has been found to be non-trivial. It has the stabilizing effect at larger values of the Reynolds number, whereas at the onset of the instability, the role is destabilizing which may be because of the increase in dynamic wave speed by the wall slip. Competing impressions of shear-thinning/shear-thickening and wall slip velocity on the primary instability are captured. The impact of slip velocity on the traveling-wave solutions is discussed using the bifurcation diagram. An increasing value of the slip shows a significant effect on the traveling wave and free surface amplitude. Slip velocity controls both the kinematic and dynamic waves of the system, and thus, it has the profound passive impact on the instability.

Published under license by AIP Publishing. <https://doi.org/10.1063/1.5078450>

NOMENCLATURE

α_1	Dimensionless parameter dependent on the substrate	\bar{h}_N	Uniform film thickness
β	Dimensionless slip parameter	κ	Permeability of the substrate
c	Phase speed	$l_c = (\sigma / (\rho g \sin \theta))^{1/2}$	Capillary length
$\cot \theta$	Slope coefficient	$l_v = (\mu_n / \rho)^{2/(n+2)} (g \sin \theta)^{(n-2)/(n+2)}$	Viscous gravity length scale
D_{ij}	Rate of strain tensor	$l_s = (\sqrt{\kappa} / \alpha_1)$	Dimensional slip length
ϵ	Film parameter	λ	Wavelength
f	Frequency	μ	Apparent viscosity
Fr	Froude number	μ_{eff}	Effective viscosity
g	Gravity acceleration	μ_n	Viscosity
$\dot{\gamma}$	Strain rate	n	Power-law index
$\Gamma = (l_c / l_v)^2$	Kapitza number	ν	Kinematic viscosity
h	Film thickness	ω	Angular frequency
h_N	Nusselt film thickness	p	Pressure
		$q = \int_0^h u dy$	Local flow rate
		Re	Reynolds number
		ρ	Density
		s	Threshold

σ	Surface tension
$t_v = (\mu_n/\rho)^{1/(n+2)}(g \sin \theta)^{-2/(n+2)}$	Viscous gravity time scale
τ	Shear stress
θ	Angle of inclination
V	Free surface velocity
We	Weber number

I. INTRODUCTION

Since the pioneering experiments by Kapitza and Kapitza,¹ many researchers have devoted their work theoretically, experimentally, and numerically to investigate the significant features of the gravity-driven thin film flow of Newtonian and non-Newtonian fluids down an inclined substrate.²⁻¹⁹ Pascal²⁰ studied the stability characteristics of a Newtonian thin film flow within the framework of the Orr-Sommerfeld analysis and showed the effect of the porous/slippy substrate on the primary instability is nontrivial. He modeled a fluid film flow over an inclined porous substrate with the Navier-slip boundary condition $u = l_s u_y$, where l_s is the effective slip length and u and u_y are, respectively, the tangential velocity and velocity gradient, equivalent to Beavers and Joseph's²¹ boundary condition ($l_s = \sqrt{\kappa}/\alpha_1$; here, κ is the permeability of the substrate and α_1 is a substrate constant). The Navier-slip boundary condition states that the velocity at the boundary is proportional to the tangential component of the wall stress. Beavers and Joseph²¹ proposed a semi-empirical velocity slip boundary condition while analyzing the macroscopic model of transport phenomena over a fluid and a permeable medium interface. Later, Sadiq and Usha²² retrieved the result of Pascal²⁰ by performing a weakly nonlinear stability analysis. However, these investigations depend on Benney's⁵ long-wave expansion and bound to a small Reynolds number. The surface conditions acquired by Sadiq and Usha²² and Thiele *et al.*²³ experience the ill effects of the finite time explode issue raised by Pumir *et al.*²⁴

Furthermore, there are many settings and applications, for example, lubrication,³⁷ microfluidics,^{25,26} and polymer melt,^{27,28} where the velocity of a viscous fluid shows a tangential slip on the substrate. Indeed, the slip impacts have been investigated in a plane Poiseuille flow with both symmetric and asymmetric slip boundary conditions.^{29,30} Lauga and Cossu³⁰ performed linear stability analysis on the pressure-driven channel flow where their results show that the presence of the slip increases the critical Reynolds number for instability, whereas Sahu *et al.*³¹ showed that the substrate slip has a destabilizing in a film flow through a diverging channel at a low Knudsen number. The presence of the wall slip on a microchannel flow of the two immiscible fluids separated by a sharp interface demonstrates the enhancement in the stability of the stratified film flow.³²

Miksis and Davis³³ determined an influential boundary condition for a single-phase film flow over a rough surface where the Navier-slip boundary condition with the slip-coefficient is equal to the average amplitude of the roughness, only if the roughness amplitude is small. Min and Kim³⁴ discussed the impacts of hydrophobic surfaces on falling film

stability and transition to turbulence in the perspective of its significance in numerous engineering applications. They represented the hydrophobic surface as a surface with the slip boundary condition, and their results successfully reveal that the slip boundary condition has a significant impact on the film stability and transition. Since the presence of the slip influences the gravity-driven film flow, several studies have been performed dealing with the slip effects.³⁵⁻⁵⁰ The mechanism of the primary instability for a film down a slippery incline has been introduced by Samanta *et al.*⁵⁰ using the Whitham wave hierarchy. They showed that the instability of the flow system is generated due to the faster propagation of kinematic waves than the dynamic waves. The slip at the wall decelerates the dynamic waves to stabilize the base flow and thus contributes to the flow system instability. At a large Reynolds number, the slip at the wall accelerates the base flow; the film thickness decreases far from the instability threshold, and the surface tension effect becomes dominant, and, consequently, the effect of the slip stabilizes beyond the threshold for instability. These studies are very relevant and significant since, in many natural and industrial settings, the bottom substrate is solid and permeable.

Mahmoud⁴⁷ investigated the wall slip and the heat generation effects in a non-Newtonian power-law fluid on a moving substrate. He found that the velocity of the fluid near the substrate decreases as the value of the slip increases, but the velocity increases at a more substantial distance. The wall slip can stimulate the significant transverse flow of shear-thickening fluids in comparison with Newtonian fluids shown by Pereira.⁴⁸ However, this transverse flow is suppressed for shear-thinning fluid. Joshi and Denn⁴⁶ studied the inertialess planar contraction flow for Newtonian and inelastic non-Newtonian fluids with the wall slip. They investigated that the physical behavior of the power-law fluid changes in the presence of a slip boundary condition, which creates a curiosity about the effect of the slip boundary on the instability of such a flow.

The wave dynamics of a falling film flow over a solid/rough surface with the slip effect has been studied previously; however, there is still a scope of improvement in the falling film wave dynamics, particularly, the wave-to-wave interaction state. However, the experimental results of Liu and Gollub⁵¹ and Vlachogiannis and Bontozoglou⁵² showed the amalgamation and repulsion events between waves which result in the number of solitary waves to decrease far from the inlet. Chang *et al.*⁵³ numerically investigated the coarsening dynamics. Moreover, it was noticed that in comparison with the Newtonian cases, non-Newtonian cases are less studied, especially for fluids with a viscous effect which is a function of the strain rate.

Recently Ruyer-Quil *et al.*^{54,55} derived a two-equation model for non-Newtonian film flows with the no-slip boundary condition at the wall to study the wave dynamics and thus the effect of wave-to-wave interaction processes by taking into account the second order $O(\epsilon^2)$ streamwise viscous diffusion effect. They successfully captured the onset of instability

and the damping of the capillary waves in a non-linear regime. The two-equation model derived earlier for Newtonian film flows by Amaouche *et al.*⁵⁶ and Fernández-Nieto *et al.*⁵⁷ that are consistent up to order ϵ enabled to capture the instability threshold correctly. These phenomena would be interesting to study with the effect of a wall slip on wave dynamics of the power-law fluid system. It has been shown that the presence of the slip boundary condition influences the wave dynamics of the flow system. Therefore, in the present study, we have considered the two-equation model of Ruyer-Quil *et al.*^{54,55} with the slip effect for power-law film flows to study the wave dynamics, the effects of the slip on the flow instability, and the effective viscosity $\mu_{\text{eff}}(\dot{\gamma})$. Our study focuses on how the presence of the slip effect influences the flow instability, and the wave dynamics can be captured accurately by considering the second order $O(\epsilon^2)$ streamwise viscous diffusion effect, which is not explored previously.

The rest of the paper is organized as follows. Section II is devoted to the formulations of governing equations and their boundary conditions. The long-wave approximation is discussed in Sec. III. A coupled two-equation model based on the boundary layer approximation and weighted-residual technique is detailed in Sec. IV. Section V presents the linear stability analysis of the base flow. The results are compared and discussed in Sec. VI. Finally, the conclusions drawn from the present study are summarized in Sec. VII.

II. MATHEMATICAL MODEL

We consider a two-dimensional power-law liquid film flowing over a slippery (or hydrophobic) inclined plane under the action of gravity, as shown in Fig. 1. The study discusses the modeling and stability analysis of a power-law film flow over a slippery/hydrophobic inclined wall. We include a thin Newtonian plateau (see Fig. 1) at a small strain rate on the top of the power-law layer to control the divergence of the effective viscosity at a zero strain rate.^{54,55} Following the work of Ruyer-Quil *et al.*,^{54,55} we also aim to model the power-law falling film over a slippery wall by taking the second order viscous diffusion term in a consistent way. Such a modeling is very helpful to easily handle the mathematical and numerical difficulties of power-law flow problems.

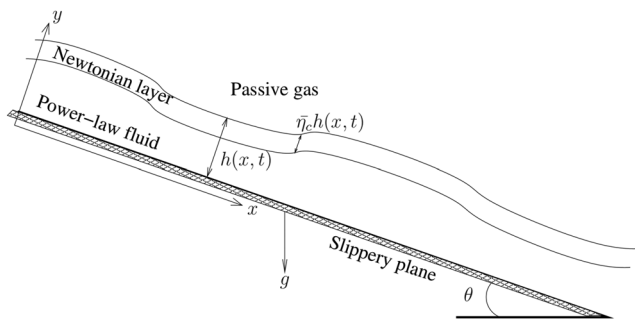


FIG. 1. Schematic diagram of a power-law film falling down over a slippery inclined plane.

The flow is assumed to be incompressible, and the fluid properties which are density ρ , surface tension σ , viscosity μ_n , power-law index n , the angle of inclination θ , and the gravity acceleration g are constant. Kinematic viscosity is denoted by $\nu = \mu_n/\rho$. A Cartesian coordinate system (x, y) is chosen along the stream-wise and cross-stream directions of the flow, respectively. Pressure p is acting inside the fluid film, and velocity components u and v are taken in the stream-wise and cross-stream directions, respectively. All the important parameters are listed in nomenclature. The dimensional form of governing equations reads as

$$\partial_x u + \partial_y v = 0, \tag{1a}$$

$$\rho(\partial_t u + u\partial_x u + v\partial_y u) = -\partial_x p + \rho g \sin \theta + \partial_x \tau_{xx} + \partial_y \tau_{xy}, \tag{1b}$$

$$\rho(\partial_t v + u\partial_x v + v\partial_y v) = -\partial_y p - \rho g \cos \theta + \partial_x \tau_{yx} + \partial_y \tau_{yy}, \tag{1c}$$

$$\text{where } \tau_{ij} = 2\mu_{\text{eff}}(\dot{\gamma})D_{ij}. \tag{1d}$$

Here, $\mathbf{u} = u\mathbf{i} + v\mathbf{j}$ is the velocity vector, $D_{ij} = (\partial_i u_j + \partial_j u_i)/2$ is the rate of strain tensor, $\dot{\gamma} = \sqrt{2D_{kl}D_{kl}}$ is the strain rate, and μ_{eff} is the effective viscosity which is a function of the strain rate $\dot{\gamma}$. The strain to shear relation

$$\mu_{\text{eff}}(\dot{\gamma}) = \mu_n \dot{\gamma}^{n-1} \tag{2}$$

is used to model the pseudo-plastic or shear-thinning fluids ($n < 1$) and dilatant or shear-thickening fluids ($n > 1$). To account for the streamwise viscous diffusion, Ruyer-Quil *et al.*^{54,55} computed the effective viscosity $\mu_{\text{eff}}(\dot{\gamma})$ and its derivative at the free surface (where $\dot{\gamma} \rightarrow 0$ for an unperturbed interface). However, for the power-law case, it was found that both the effective viscosity and its derivative at $\dot{\gamma} = 0$ are undefined for the power-law index $n < 3$, which corresponds to mostly the shear-thinning and shear-thickening fluids. This circumstance requires a regularization at the zero strain rate of the power-law by introducing the Newtonian layer at the low strain rates.

A regularization of the Ostwald-de Waele power law model [Eq. (2)] is assumed at the reduced shear rate to regain the Newtonian characteristic in the proper limit. The three-parameter Carreau law is given as

$$\mu_{\text{eff}}(\dot{\gamma}) = \mu_0 \left[1 + \left(\frac{\dot{\gamma}}{\dot{\gamma}_c} \right)^2 \right]^{\frac{(n-1)}{2}},$$

where μ_0 is the zero strain viscosity near the free surface and $\dot{\gamma}_c$ is the critical strain rate separating Newtonian and non-Newtonian behaviors of shear-thinning xanthan dilute solutions. However, using the above relation forbids the base flow from being determined analytically and one can instead introduce a Newtonian plateau,

$$\mu_{\text{eff}}(\dot{\gamma}) = \begin{cases} \mu_n \dot{\gamma}^{n-1}, & \text{for } \dot{\gamma} > \dot{\gamma}_c \\ \mu_0, & \text{for } \dot{\gamma} \leq \dot{\gamma}_c \end{cases}.$$

The system of Eq. (1) is closed by the boundary conditions prescribed at the free surface $y = h(x, t)$,

$$\left[1 - (\partial_x h)^2\right] \tau_{xy} + \partial_x h (\tau_{yy} - \tau_{xx}) = 0, \quad (3a)$$

$$p_a - p + \frac{\tau_{xx}(\partial_x h)^2 - 2\tau_{xy}\partial_x h + \tau_{yy}}{1 + (\partial_x h)^2} = \frac{\sigma \partial_{xx} h}{[1 + (\partial_x h)^2]^{3/2}}, \quad (3b)$$

$$\partial_t h + u \partial_x h = v, \quad (3c)$$

and at the wall $y = 0$

$$u = \frac{\sqrt{\kappa}}{\alpha_1} u_y \quad \text{and} \quad v = 0, \quad (3d)$$

where κ is the permeability of the substrate and α_1 is a dimensionless parameter dependent on the substrate.

Using the viscous-gravity length $l_v = (\mu_n/\rho)^{2/(n+2)} (g \sin \theta)^{(n-2)/(n+2)}$ and the time scale $t_v = \left(\frac{\mu_n}{\rho}\right)^{\frac{1}{n+2}} (g \sin \theta)^{-\frac{2}{n+2}}$, the non-dimensional form of governing equations reads as

$$u_x + v_y = 0, \quad (4a)$$

$$Re(u_t + uu_x + vv_y) = -p_x + 1 + \tau_{xxx} + \tau_{xyy}, \quad (4b)$$

$$Re(v_t + uv_x + vv_y) = -p_y - \cot \theta + \tau_{yxx} + \tau_{yyx}. \quad (4c)$$

Note that the viscous-gravity length scale l_v is defined based on the balance of gravity acceleration and viscous drag.^{10,54,55} However, the balance of viscosity and gravity acceleration corresponds to the viscous-gravity time scale t_v . The dimensionless boundary conditions along with the above governing equations are: (i) The Navier-slip boundary condition¹⁵ and the no-penetration condition at the plane, $y = 0$,

$$u = \beta u_y, \quad v = 0, \quad (4d)$$

where $\beta = l_s/l_v$ is the dimensionless slip length ($l_s = \sqrt{\kappa}/\alpha_1$). (ii) The balance of tangential and normal stresses at the free surface, $y = h(x, t)$,

$$\left[1 - (h_x)^2\right] \tau_{xy} + h_x (\tau_{yy} - \tau_{xx}) = 0, \quad (4e)$$

$$-p + \frac{\tau_{xx}(h_x)^2 - 2\tau_{xy}h_x + \tau_{yy}}{1 + (h_x)^2} = We \frac{h_{xxx}}{[1 + (h_x)^2]^{3/2}}, \quad (4f)$$

(iii) The kinematic boundary condition at the free surface, $y = h(x, t)$,

$$h_t + uh_x = v. \quad (4g)$$

The Weber number is defined as $We = \sigma/(\rho g \sin \theta \bar{h}_N^2)$. Finally, surface tension, gravity, and viscous drag can be written as a function of the Kapitza number,

$$\Gamma = (l_c/l_v)^2 = (\sigma/\rho)(\mu_n/\rho)^{-4/(n+2)} (g \sin \theta)^{(2-3n)/(n+2)}, \quad (5)$$

where $l_c = \sqrt{[\sigma/(\rho g \sin \theta)]}$ is the capillary length. The Weber and Kapitza numbers can be related by the relation $We = \Gamma(l_v/\bar{h}_N)^2$.

The velocity scale V is defined by

$$V = \left(\frac{\rho g \bar{h}_N^{n+1} \sin \theta}{\mu_n}\right)^{1/n} \left[1 + \beta \frac{n+1}{n}\right], \quad (6)$$

where \bar{h}_N , the uniform film thickness, is the length scale. The Froude number $Fr = V/\sqrt{g \bar{h}_N \cos \theta}$, which compares the characteristic speed of the flow with the speed of the gravity waves propagating at the interface, and the Reynolds number

$$Re = \frac{\rho V^{2-n} \bar{h}_N^n}{\mu_n} = [(\mu_n/\rho)^{-2} (g \sin \theta)^{2-n} \bar{h}_N^{n+2}]^{1/n} \left[1 + \beta \frac{n+1}{n}\right]^{2-n} \quad (7)$$

are related to the Froude number by a relation $Re/\cot \theta = Fr^2$. The Reynolds number is also written as $Re = (\bar{h}_N/l_v)^{(n+2)/n} \left[1 + \beta \frac{n+1}{n}\right]^{2-n}$ which balances the gravity acceleration and viscous drag. We may also rewrite the velocity scale V as

$$V = \frac{l_v}{t_v} \left(\frac{\bar{h}_N}{l_v}\right)^{\frac{n+1}{n}} \left[1 + \beta \frac{n+1}{n}\right]. \quad (8)$$

Note that the term with β is coming due to the wall velocity slip.

III. LONG-WAVE EXPANSION

We assume (i) slow space and time evolutions $\partial_{x,t} \sim \epsilon$ where $\epsilon \ll 1$ is a formal film parameter and (ii) surface deformations induce order- ϵ correction of the velocity profile from the flat-film solution. Otherwise stated, assumption (ii) implies that viscosity is strong enough to ensure the cross-stream coherence of the flow which should be verified for small to moderate Reynolds numbers ($Re \sim O(1)$). Following the long-wave expansion technique, we can write

$$u = u_0 + \epsilon u_1 + \epsilon^2 u_2 \dots, \quad v = \epsilon v_1 + \epsilon^2 v_2 \dots, \quad p = p_0 + \epsilon p_1 + \epsilon^2 p_2 \dots, \quad (9)$$

$$\tau_{yx} = u_0 y^n + \epsilon(n),$$

$$\begin{aligned} \tau_{xx} &= 2\partial_x u \left[2(\partial_x u)^2 + (\partial_y u + \partial_x v)^2 + 2(\partial_y v)^2\right]^{(n-1)/2} \\ &= 2\partial_x u_0 |\partial_y u_0|^{n-1} + O(\epsilon^3), \end{aligned}$$

$$\begin{aligned} \tau_{yy} &= 2\partial_y v \left[2(\partial_x u)^2 + (\partial_y u + \partial_x v)^2 + 2(\partial_y v)^2\right]^{(n-1)/2} \\ &= 2\partial_y v_0 |\partial_y u_0|^{n-1} + O(\epsilon^3). \end{aligned}$$

Integrating Eq. (4a) with respect to y and using kinematic boundary condition (4g), the equation regarding mass balance is obtained as

$$h_t + \left(\int_0^h u dy\right)_x = h_t + q_x = 0, \quad (10)$$

where $q(x, t) = \int_0^h u dy$ is the local flow rate. Substituting (9) into (4a)–(4f), we consider the zeroth-order equations and boundary conditions of $O(\epsilon^0)$,

$$\begin{aligned} (u_0 y^n)_y + 1 &= 0, \quad p_0 y + \cot \theta = 0, \quad u_0 = \beta u_{0y}, \\ u_0 y^n|_{h=0} &= 0, \quad p_0 = -We h_{xxx}. \end{aligned} \quad (11)$$

The term Weh_{xxx} represents the capillary force that prevents the breaking of nonlinear waves.¹³ The solutions of the zeroth-order equations are given by

$$u_0 = \frac{n}{n+1} h^{\frac{n+1}{n}} \left\{ \left[1 - \left(1 - \frac{y}{h} \right)^{\frac{n+1}{n}} \right] + \frac{\beta}{h} \right\}, \quad p_0 = \cot \theta (h - y) - Weh_{xxx}, \quad (12)$$

and the corresponding flow rate becomes

$$q(x, t) = \frac{n}{1+2n} h^{\frac{1+2n}{n}} + \beta h^{\frac{n+1}{n}}, \quad (13)$$

which depicts the dependency of the flow to the kinematics of the free surface elevation. Substituting $q(x, t)$ from (13) into the mass conservation Eq. (10), we obtain the following nonlinear hyperbolic wave equation:⁶⁴

$$h_t + \left(h^{\frac{1+n}{n}} + \frac{n+1}{n} \beta h^{\frac{1}{n}} \right) h_x = 0. \quad (14)$$

Solving for the perturbation fields $u_1, v_1,$ and p_1 at order ϵ , the consistent surface equation at that order is

$$h_t + \left[h^{\frac{1+n}{n}} \frac{\beta + 2n\beta + nh}{1+2n} \right]_x + \left[Reh^{\frac{3}{n}} \frac{\beta + nh}{n^3(2+7n+6n^2)} \right. \\ \times \{ (2+7n+6n^2)\beta^2 + 2nh(2+3n)\beta + 2n^2h^2 \} h_x \\ \left. - h^{\frac{1+n}{n}} \frac{(2+3n)(\beta + 2n\beta + nh)}{n(2+7n+6n^2)} (\cot \theta h_x - Weh_{xxx}) \right]_x = 0. \quad (15)$$

We consider a uniform solution $h(x, t) = h_N + \eta(x, t)$ of (15), where $\eta(x, t)$ is an infinitesimal disturbance from the base state solution. Substituting the expression for $h(x, t)$ into Eq. (15) and linearizing the resulting equation, we obtain

$$\eta_t + A(h_N)\eta_x + B(h_N)\eta_{xx} - C(h_N)(\cot \theta \eta_{xx} - We\eta_{xxxx}) = 0, \quad (16a)$$

where

$$A(h_N) = \frac{1}{2n+1} \left[nh_N^{\frac{1+n}{n}} + \frac{1+n}{n} h_N^{\frac{1}{n}} (\beta + 2n\beta + nh_N) \right], \quad (16b)$$

$$B(h_N) = Reh_N^{\frac{3}{n}} \frac{\beta + nh_N}{n^3(6n^2 + 7n + 2)} \left[(6n^2 + 7n + 2)\beta^2 + 2nh_N(3n + 2)\beta + 2n^2h_N^2 \right], \quad (16c)$$

$$C(h_N) = \frac{(3n+2)(nh_N + \beta + 2n\beta)}{n(6n^2 + 7n + 2)}. \quad (16d)$$

Now linearizing (16a) with $\eta(x, t) = e^{i(x-ct)}$ and then calculating the value of $C = C_r + iC_i$, where $C_r = (1 + \beta \frac{n+1}{n})$ and $C_i = 0$, the neutral stability condition with a critical Reynolds number can be obtained as

$$Re_c = \frac{n^2(3n+2)(n+\beta+2n\beta)}{(n+\beta)[2n^2+n\beta(6n+4)+\beta^2(6n^2+7n+2)]} \cot \theta. \quad (17)$$

Notably the zeroth, first order solutions and C_r and Re_c are all dependent on the slip parameter. One can easily recover the critical Re value for the Newtonian liquid film down a no-slip inclined wall by putting the slip parameter $\beta = 0$ and the power-law index $n = 1$ in Eq. (17), which give Re_c for our problem. Substituting $\beta = 0$ and $n = 1$ in Eq. (17), we get $Re_c = \frac{5}{2} \cot \theta$ for a Newtonian falling film, which is exactly three times of the critical Reynolds number calculated by Yih.¹⁹ Using the average velocity of the film $U_a = gh_N^2 \sin \theta / 3\nu$ as the velocity scale, Yih found $Re_c = \frac{5}{6} \cot \theta$ in the classical case.¹⁹ In the current work, we have used the free surface velocity $V = gh_N^2 \sin \theta / \nu$ (for $\beta = 0, n = 1$) as the velocity scale which is $\frac{1}{3}$ times of the average velocity (i.e., $U_a = 3V$). Thus, our Re_c in the classical case¹⁹ is exactly three times of Yih's critical Re .

IV. DEPTH-AVERAGED MODEL

Assumption (i) from Sec. III with the continuity equation renders the cross-stream velocity $v = -\int_0^y u_x dy = O(\epsilon)$ so that the inertia term can be truncated from the cross-stream momentum equation which produces the pressure distribution at order ϵ after integration,

$$\text{if } y > y_c, \quad p = \cot \theta (h - y) - Weh_{xxx} - r[u_x|_h + u_x], \quad (18a)$$

$$\text{if } y \leq y_c, \quad p = \cot \theta (h - y) - Weh_{xxx} - r[u_x|_h + u_x|_{y_c}] \\ + 2ru_x|_{y_c} - 2u_x\gamma_0^{n-1} - \int_y^{y_c} [u_y\gamma_0^{n-1}]_x dy, \quad (18b)$$

where $y_c = h(1 - \bar{\eta}_c)$ defines the location of the imaginary interface separating the Newtonian and power-law layers and $\gamma_0 = \sqrt{(u_y)^2 + 4(u_x)^2}$. Then, substituting Eq. (18) into the stream-wise momentum balance gives

$$Re(u_t + uu_x + vv_y) = 1 + \tau_{xy}^{(0)} + \mathcal{D}^{(2)} - \cot \theta h_x + Weh_{xxx}, \quad (19a)$$

where both the lowest order rate of strain $\tau_{xy}^{(0)}$ and the second-order viscous terms $\mathcal{D}^{(2)}$ depend on Newtonian and non-Newtonian fluids. For $y > y_c$, they read

$$\tau_{xy}^{(0)} = ru_y \quad \text{and} \quad \mathcal{D}^{(2)} = 2ru_{xx} + r[\partial_x u|_h]_x, \quad (19b)$$

whereas for $y \leq y_c$, we have

$$\tau_{xy}^{(0)} = u_y\gamma_0^{n-1}, \\ \mathcal{D}^{(2)} = [v_x(\gamma_0^{n-1} + (n-1)(u_y)^2\gamma_0^{n-3})]_y + 4[u_x\gamma_0^{n-1}]_x \\ + \left\{ \int_y^{y_c} [u_y\gamma_0^{n-1}]_x dy \right\}_x - 2[ru_x|_{y_c}]_x + r[u_x|_{y_c} + u_x|_h]_x, \quad (19c)$$

which are completed by the slip velocity condition at the wall ($y = 0$) and the tangential, normal stresses continuity at the free surface $y = h(x, t)$, truncated at order ϵ^2 ,

$$u_y = 4h_x u_x - v_x. \tag{19d}$$

Let us consider that the assumption (ii) of Sec. III holds, implying the velocity approximation over the fluid layer is never far from the flat film solution. This can be expressed by

$$u = u_s + \tilde{u}^{(l)}, \quad \text{where} \tag{20a}$$

$$u_s = \bar{u}f_0(\bar{y}) \quad \text{for} \quad \bar{y} \leq 1 - \bar{\eta}_c, \tag{20b}$$

$$u_s = \bar{u} \left[f_0(1 - \bar{\eta}_c) + \bar{\eta}_c^{(n+1)/n} g_0[(\bar{y} + \bar{\eta}_c - 1)/\bar{\eta}_c] \right] \quad \text{for} \quad \bar{y} \geq 1 - \bar{\eta}_c, \tag{20c}$$

and $\bar{\eta}_c$ is the local relative thickness of the Newtonian layer at the free surface. The definition of the velocity approximation u_s is based on the local film thickness $h(x, t)$ and a local velocity scale $\bar{u}(x, t)$ that can be related to the rate of strain at the wall $D_{xy}|_{y=0} = \bar{u}/h + O(\epsilon)$. Here, $\tilde{u}^{(l)}$ accounts for $O(\epsilon)$ deviations of the velocity profile induced by the deformation of the free surface. The $O(\epsilon)$ corrections of the relation between the flow rate $q = \int_0^h u \, dy$, h , and \bar{u} provided below by the flat-film profile

$$q = \frac{3(n + \beta + 2n\beta) + (1 - n)\bar{\eta}_c^{-(2n+1)/n}}{6n + 3} h \bar{u} \equiv \phi(\bar{\eta}_c) h \bar{u} \tag{21}$$

can also be included into $\tilde{u}^{(l)}$ so that $\int_0^h \tilde{u}^{(l)} \, dy = 0$ is assumed without any restriction.

The local thickness $\bar{\eta}_c$ of the Newtonian layer is defined by $\bar{y}(\bar{y} = 1 - \bar{\eta}_c) = s$, which reads at order ϵ^2 as

$$s^2 = \left\{ 4(u_{sx})^2 + [u_{sy} + v_{sx}]^2 \right\}_{\bar{y}=1-\bar{\eta}_c}. \tag{22}$$

In the limit $\bar{\eta}_c \ll 1$, (22) can be further simplified to yield

$$s^2 = \frac{4n^2}{(1+n)^2} (\bar{u}_x)^2 + \bar{\eta}_c^{2/n} \frac{\bar{u}^2}{h^2}. \tag{23}$$

Hence, the Newtonian layer disappears locally if

$$|\bar{u}_x| > \frac{n+1}{2n} s. \tag{24}$$

We have implemented the weighted residual technique and averaged the boundary-layer Eqs. (19) across the film flow (see Ruyer-Quil et al.^{54,55} for details). Now, we introduce a weighting function $w(\bar{y})$ and the scalar product $\langle \cdot | \cdot \rangle = \int_0^h \cdot \, dy$. An equation of $O(\epsilon)$ consistency can be obtained by choosing the weight w in such a way that the viscous drag term

$$\begin{aligned} & \int_0^{y_c} w(\bar{y}) [n|u_{sy}|^{n-1} \tilde{u}^{(l)}_{,y}] \, dy + \int_{y_c}^h r w(\bar{y}) \tilde{u}^{(l)}_{,yy} \, dy \\ & \equiv \frac{1}{h} \left| \frac{\bar{u}}{h} \right|^{n-1} \langle \mathcal{L}_{\bar{\eta}_c} \tilde{u}^{(l)} | w \rangle + O(\epsilon^2) \end{aligned} \tag{25}$$

is of order ϵ^2 . The linear operator $\mathcal{L}_{\bar{\eta}_c}$ is defined as

$$\mathcal{L}_{\bar{\eta}_c} = \partial_{\bar{y}} [n(f'_0)^{n-1} \partial_{\bar{y}} \cdot] \quad \text{if} \quad 0 \leq \bar{y} \leq \bar{\eta}_c,$$

and

$$\mathcal{L}_{\bar{\eta}_c} = \bar{\eta}_c^{(n-1)/n} \partial_{\bar{y}\bar{y}} \cdot \quad \text{otherwise,} \tag{26}$$

where the thickness of the Newtonian layer is estimated by $\bar{\eta}_c = (sh/\bar{u})^n + O(\epsilon^2)$.

Two integrations by part of Eq. (25) show that the linear operator $\mathcal{L}_{\bar{\eta}_c}$ is self-adjoint. We can make use of $q(\int_0^h u^{(l)} \, dy = 0)$ in such a way that the weight function w must be a solution to $\mathcal{L}_{\bar{\eta}_c} = \text{constant}$, thereby yielding

$$\text{if } y < y_c, \quad w(\bar{y}) = f_0(\bar{y}), \tag{27a}$$

$$\text{if } y \geq y_c, \quad w(\bar{y}) = f_0(1 - \bar{\eta}_c) + n\bar{\eta}_c^{(n+1)/n} g_0[(\bar{y} + \bar{\eta}_c - 1)/\bar{\eta}_c]. \tag{27b}$$

It is noteworthy to mention that the weight w is not proportional to the velocity profile u_s . The weighted residual method considered here is therefore slightly different from the Galerkin method such that $w \propto u_s$. This discrepancy is an impact of the nonlinearity of the strain to stress relationship which presents a factor n . Then, we proceed to the averaging of the boundary-layer Eqs. (19) with appropriate weights (27). We expand the nonlinear constitutive equation to compute the viscous terms appearing in the boundary-layer formulation (19c),

$$\dot{\gamma}_0^{n-1} = |u_y|^{n-1} + 2(n-1)(u_x)^2 |u_y|^{n-3} + O(\epsilon^4), \tag{28}$$

and replace r with $\dot{\gamma}_0^{n-1}|_{y=h(1-\bar{\eta}_c)}$.

The resulting averaged momentum Eq. (19) reads

$$\begin{aligned} \bar{u}_t = & -Re \left[\tilde{G} \frac{\bar{u}^2}{h} h_x + \tilde{F} \bar{u} \bar{u}_{xx} \right] + \tilde{I} \left(1 - \cot \theta h_x + We h_{xxx} - \frac{\bar{u} |\bar{u}|^{n-1}}{h^{n+1}} \right) \\ & + \tilde{J} \frac{\bar{u}}{h^2} (h_x)^2 + \tilde{K} \frac{\bar{u}_x h_x}{h} + \tilde{L} \frac{\bar{u}}{h} h_{xxx} + \tilde{M} \bar{u}_{xxx} + \tilde{N} \frac{(\bar{u}_x)^2}{\bar{u}}. \end{aligned} \tag{29}$$

The coefficients \tilde{F} to \tilde{N} of (29) are explicit, but they are ponderously functions of n, β , and of the relative thickness $\bar{\eta}_c$ of the Newtonian layer. The full expressions of the coefficients \tilde{F}, \tilde{G} , and \tilde{I} of the terms of orders ϵ^0 and ϵ are provided in Appendix A which will be useful to compose the value of the critical Reynolds number at onset. The system of Eqs. (10), (22), and (29) is consistent up to order ϵ and precisely computed for second-order viscous terms. The derivation of Eq. (29) has required a regularization of (2) for $n < 3$, especially to compute both $\mu_{\text{eff}}(0)$ and $d\mu_{\text{eff}}/d\dot{\gamma}(0)$ in (28). The full derivation of the averaged momentum balance (29) for the generalized Newtonian fluid⁶⁵ with no-slip was provided by Ruyer-Quil et al.^{54,55}

A. Shear-thinning film ($n < 1$)

Equations (10), (22), and (29) are still inextricable to solve because of the coefficient (Appendix A) dependency on the relative thickness $\bar{\eta}_c$ of the Newtonian layer, which is thus a nonlinear function of h, \bar{u} , and their derivatives. Therefore, we further simplify the formulation by maintaining the asymptotic behavior of the coefficients when the Newtonian layer is very thin (i.e., $\bar{\eta}_c \rightarrow 0$).

In this limit, q can be easily substituted for \bar{u} . After some algebraic calculation, we finally obtain

$$Re q_t = Re \left[-F(n) \frac{q}{h} q_x + G(n) \frac{q^2}{h^2} h_x \right] + I(n) \left[h(1 - \cot \theta h_x + We h_{xxx}) - \frac{q|q|^{n-1}}{(\phi_0 h^2)^n} \right] + r \left[J_0(n) \frac{q}{h^2} (h_x)^2 - K_0(n) \frac{q_x h_x}{h} - L_0(n) \frac{q}{h} h_{xx} + M_0(n) q_{xx} \right], \tag{30}$$

where $\phi_0 = \phi(0) = n/(2n + 1) + \beta$. The coefficients $F(n)$, $G(n)$, \dots , $M_0(n)$ are also functions of n and β whose expressions are given below,

$$F = \frac{[2n^3(11n + 6) + n^2\beta(4n + 3)(23n + 12) + 6n\beta^2(2n + 1)(3n + 2)(4n + 3) + 2\beta^3(2n + 1)^2(3n + 2)(4n + 3)]}{(4n + 3)(n + \beta + 2n\beta)[2n^2 + 2n\beta(3n + 2) + \beta^2(6n^2 + 7n + 2)]}, \tag{31a}$$

$$G = \frac{(2n + 1)[6n^3 + 6n^2\beta(4n + 3) + 3n\beta^2(3n + 2)(4n + 3) + \beta^3(2n + 1)(3n + 2)(4n + 3)]}{(4n + 3)(n + \beta + 2n\beta)[2n^2 + 2n\beta(3n + 2) + \beta^2(6n^2 + 7n + 2)]}, \tag{31b}$$

$$I = \frac{(3n + 2)(n + \beta + 2n\beta)^2}{(2n + 1)[2n^2 + 2n\beta(3n + 2) + \beta^2(6n^2 + 7n + 2)]}, \tag{31c}$$

$$K_0 = J_0 = -\frac{2n^2(n - 1)(2n + 1)(3n + 2)(n + \beta + n\beta)}{(n + 1)^2(n + \beta + 2n\beta)[2n^2 + 2n\beta(3n + 2) + \beta^2(6n^2 + 7n + 2)]}, \tag{31d}$$

$$L_0 = K_0/2, \quad M_0 = -\frac{(n - 1)(3n + 2)(n + \beta + n\beta)(n + \beta + 2n\beta)}{(n + 1)[2n^2 + 2n\beta(3n + 2) + \beta^2(6n^2 + 7n + 2)]}. \tag{31e}$$

Still, under the limit of a thin layer of Newtonian fluid, the strain-rate threshold s is expected to go toward zero. Thus, the Newtonian layer can be easily removed by $O(s)$ gradients h_x of the film thickness [computed from (24)]. In that case, the effective viscosity $\mu_{\text{eff}}(y = h)$ at the free surface is much smaller than its maximum r . The streamwise viscous effects are consequently overestimated by (30) at whatever point the free surface is non-weakly distorted. To correctly estimate these viscous effects, one must consider those film regions where the effective viscosity reaches its maximum. Moreover, at the free surface, the contributions of the effective viscosity to the streamwise viscous diffusion

terms of the averaged momentum balance can be easily computed by substituting r for the effective viscosity $\mu_{\text{eff}}(y = h)$ into (29). However, it is a difficult task to compute the leading contributions of the bulk and wall regions to the streamwise viscous diffusion terms of the averaged momentum balance. A straightforward but unique way to proceed with the analysis is to evaluate the effective viscosity in the bulk region from its value at the wall $\mu_{\text{eff}}(y = 0) \approx [q|q|/(\phi_0 h^2)]^{n-1} = h^{(n-1)/n} + O(\epsilon)$, expect a consistent viscosity inside the layer and calculate the $O(\epsilon^2)$ viscous contribution to the averaged momentum equation (see Appendix B of Ruyer-Quil et al.^{54,55}). Then, we obtain

$$Re q_t = Re \left[-F(n) \frac{q}{h} q_x + G(n) \frac{q^2}{h^2} h_x \right] + I(n) \left[h(1 - \cot \theta h_x + We h_{xxx}) - \frac{q|q|^{n-1}}{(\phi_0 h^2)^n} \right] + r(h, q) \left[J_0(n) \frac{q}{h^2} (h_x)^2 - K_0(n) \frac{q_x h_x}{h} - L_0(n) \frac{q}{h} h_{xx} + M_0(n) q_{xx} \right] + h^{(n-1)/n} \left[J_w(n) \frac{q}{h^2} (h_x)^2 - K_w(n) \frac{q_x h_x}{h} - L_w(n) \frac{q}{h} h_{xx} + M_w(n) q_{xx} \right], \tag{32}$$

where J_w , K_w , L_w , and M_w are defined as

$$J_w = \frac{2[n^2(3n^2 + 13n + 8) + n\beta(15n^3 + 52n^2 + 52n + 16) + \beta^2(12n^4 + 50n^3 + 70n^2 + 40n + 8)]}{(n + 2)(n + 1)[2n^2 + 2n\beta(3n + 2) + \beta^2(6n^2 + 7n + 2)]}, \tag{33a}$$

$$K_w = M_w = \frac{2[n^2(5n + 4) + n\beta(15n^2 + 22n + 8) + \beta^2(12n^3 + 26n^2 + 18n + 4)]}{(n + 1)[2n^2 + 2n\beta(3n + 2) + \beta^2(6n^2 + 7n + 2)]}, \tag{33b}$$

$$L_w = \frac{[n^2(17n^2 + 23n + 8) + n\beta(39n^3 + 89n^2 + 66n + 16) + \beta^2(24n^4 + 76n^3 + 88n^2 + 44n + 8)]}{(n + 1)^2[2n^2 + 2n\beta(3n + 2) + \beta^2(6n^2 + 7n + 2)]}, \tag{33c}$$

and $r(h, q)$ refers the evaluation of the effective viscosity at the free surface $\mu_{\text{eff}}(y = h)$ from h and q ,

$$r(h, q) \equiv [s^2 + v_{s,x}^2 + 4(u_{s,xx})^2]^{(n-1)/2} \Big|_{y=h}, \tag{34a}$$

where

$$v_{s,x}^2 + 4(u_{s,xx})^2 \Big|_{y=h} = \left[\frac{2(2n+1)}{n+1} \left(\frac{q}{h} \right)_x \right]^2 + \left\{ \frac{2n+1}{n+1} \left[-2 \frac{h_x q_x}{h} + q \left(2 \frac{(h_x)^2}{h^2} - \frac{h_{xx}}{h} \right) \right] + q_{xx} \right\}^2. \tag{34b}$$

The averaged momentum equation derived by Ruyer-Quil and Manneville¹⁷ can be retrieved by substituting $n = 1$ and $\beta = 0$ into (32) for the Newtonian case with the no-slip condition.

B. Shear-thickening film ($n > 1$)

In shear-thickening case, preventing the leading order terms in the limit of $s \rightarrow 0$, the averaged momentum Eq. (29) reduces to (for $1 < n < 3$)

$$\text{Re}q_t = \text{Re} \left[-F(n) \frac{q}{h} q_x + G(n) \frac{q^2}{h^2} h_x \right] + I(n) \left[h(1 - \cot \theta h_x + \text{We} h_{xxx}) - \frac{q|q|^{n-1}}{(\phi_0 h^2)^n} \right] + \left[\frac{|q|}{\phi_0 h^2} \right]^{n-1} \times \left[J_1(n) \frac{q}{h^2} (h_x)^2 - K_1(n) \frac{q_x h_x}{h} - L_1(n) \frac{q}{h} h_{xx} + M_1(n) q_{xx} \right]. \tag{35}$$

The coefficients are given as

$$J_1 = - \frac{(3n + 2)[n(8n^4 + 24n^3 - 8n^2 - n + 1) + 2n^2\beta(16n^3 + 52n^2 + 8n - 9) + 6n\beta^2(24n^3 + 10n^2 - 3n - 1) + \beta]}{3(2n - 1)(4n + 1)[2n^2 + n\beta(6n + 4) + \beta^2(6n^2 + 7n + 2)]}, \tag{36a}$$

$$K_1 = - \frac{n(2n + 1)(3n + 2)[n(2n + 7) + 2n\beta(4n + 15) + 12\beta^2(4n + 1) + 7\beta]}{3(4n + 1)[2n^2 + n\beta(6n + 4) + \beta^2(6n^2 + 7n + 2)]}, \tag{36b}$$

$$L_1 = \frac{(2n + 1)(3n + 2)[2n(12n^3 + 36n^2 + n - 1) + 3n\beta(24n^3 + 82n^2 + 37n + 1) + 24n\beta^2(24n^2 + 7n + 1) - 2\beta]}{6(2n - 1)(3n + 1)(4n + 1)[2n^2 + n\beta(6n + 4) + \beta^2(6n^2 + 7n + 2)]}, \tag{36c}$$

$$M_1 = \frac{n(2n + 1)(3n + 2)[2n(2n + 7) + 4n\beta(4n + 15) + 24\beta^2(4n + 1) + 14\beta]}{6(2n - 1)(4n + 1)[2n^2 + n\beta(6n + 4) + \beta^2(6n^2 + 7n + 2)]}. \tag{36d}$$

We have considered the power-law index n within the range of $1 < n < 3$ for the shear-thickening case because the rheological estimate of the parameters for shear-thickening fluids in Table I shows that the minimum and maximum values of n are 1.3 and 2.4, respectively. Moreover, the properties of the

shear-thickening fluid at $n > 3$ change and become more like a solid in nature.^{58,59} In the Newtonian limit $n \rightarrow 1$ with no-slip $\beta = 0$, the averaged momentum equation derived by Ruyer-Quil and Manneville¹⁷ can be retrieved. However, the coefficients of the stream-wise viscous diffusion terms $q(h_x)^2/h^2$ and

TABLE I. Values of parameters from rheological estimation of the xanthan gum solutions in water (sets 1, 60.61 2, and 3, 62 surface tension, $\sigma = 65$ mN/m, and density, $\rho = 995$ kg/m³) and cornstarch dispersions in ethylene glycol⁶³ (sets 4, 5, and 6, surface tension, $\sigma = 48$ mN/m, and density, $\rho = 1113$ kg/m³). The viscosity μ_0 of the Newtonian plateau is assumed to correspond to the solvent viscosity. Values of the Kapitza number are evaluated for an inclination angle $\theta = 15^\circ$.

Set number	Concentration	μ_n (Pa s ⁿ)	n	μ_0 (Pa s)	$\dot{\gamma}_c$ (s ⁻¹)	$\dot{\gamma}_c \tau_v$	Γ
1	500 ppm	0.040 62	0.607	0.08	0.18	1.8×10^{-3}	378
2	1500 ppm	0.359 2	0.40	1.43	0.1	1.7×10^{-3}	48.7
3	2500 ppm	0.991 3	0.34	7.16	0.05	1.2×10^{-3}	13.0
4	33%	8	1.3	0.016	10^{-9}	1.3×10^{-10}	0.01
5	35%	6	1.55	0.016	2.1×10^{-5}	2.8×10^{-6}	0.0077
6	38%	1.8	2.4	0.016	0.034	5.2×10^{-3}	0.005

$q_x h_x/h$ at $n = 1$ and $\beta = 0$ are as $K_1 = 9/2$ and $J_1 = 4$. It is noteworthy to mention that these terms are nonlinear and do not contribute to the linear stability analysis of the Nusselt base flow.^{54,55}

V. LINEAR STABILITY ANALYSIS

A. Orr-Sommerfeld analysis

We have considered the linear stability of the Nusselt uniform film solution in this section. We first linearize the governing Eqs. (4) with a fluid modeled by a power-law and a Newtonian behavior at a low rate of strain.^{54,55} Then, we perturb the basic state solution with $h = 1$,

$$\text{if } y < 1 - s^n, U(y) = \frac{1}{\phi(\beta)} f_0(y)$$

$$\text{else } U(y) = \frac{1}{\phi(\beta)} (f_0(1 - s^n) + s^{n+1} g_0 [s^{-n}(y + s^n - 1)]), \tag{37a}$$

$$P(y) = \cot \theta (1 - y). \tag{37b}$$

Then, introducing a stream function and decomposing it on normal modes,

$$u = U + \Re(\psi'(y)e^{ik(x-ct)}), \quad v = \Re(-ik\psi(y)e^{ik(x-ct)}),$$

$$h_i = 1 - s^n + \Re(f_i e^{ik(x-ct)}),$$

where $\phi(\beta) = (1 + \beta \frac{n+1}{n})$ and k and c are the wavenumber and phase speed, respectively. In addition, \Re stands for the real part, and h_i refers to the position of the imaginary interface separating the Newtonian and non-Newtonian regions of the flow. Then, we obtain an Orr-Sommerfeld eigenvalue problem (following the standard procedure),

$$\text{if } y < 1 - s^n, \quad ik\text{Re}[(U - c)(D^2 - k^2)\psi - \psi U'']$$

$$= (D^2 + k^2)[n(U)^{n-1}(D^2 + k^2)\psi]$$

$$- 4k^2 D[(U)^{n-1} D\psi], \tag{38a}$$

$$\text{else, } ik\text{Re}[(U - c)(D^2 - k^2)\psi - \psi U''] = r(D^2 - k^2)^2 \psi, \tag{38b}$$

where $D \equiv d/dy$ and again $r = s^{n-1}$ is the ratio of the viscosity at the free surface and at the wall. The system of equations

in (38) is closed by the boundary conditions prescribed at the wall and at the interface,

$$\psi'(0) = \beta\psi''(0), \quad \psi(0) = 0, \tag{38c}$$

$$k^2\psi(1) + \psi''(1) + U''(1)\frac{\psi(1)}{c - U(1)} = 0, \tag{38d}$$

$$\frac{\psi(1)}{\phi(\beta)(c - U(1))} (Wek^3 + \cot \theta k) + k\text{Re}[U(1) - c]\psi'(1)$$

$$+ ir[\psi'''(1) - 3k^2\psi'(1)] = 0. \tag{38e}$$

The amplitude of the deformation of the imaginary interface is given by

$$f_i = ns^{n-1}(k^2\psi|_{y_c} + \psi''|_{y_c}), \tag{38f}$$

where $y_c = 1 - s^n$ refers to the location of the interface for the base flow. The continuity of the velocity implies the continuity of ψ and ψ' at $y = y_c$. The continuity of stresses at the imaginary interface ($y_c = 1 - s^n$) leads to

$$\psi''|_{y_c} = [n\psi'' + (n - 1)k^2\psi]|_{y_c}, \tag{38g}$$

$$s^n[\psi''']|_{y_c} = \{s^n[n\psi''' + (n - 1)k^2\psi'] - (n - 1)[\psi'' + k^2\psi]\}|_{y_c}. \tag{38h}$$

We solve the system of the linearized Eqs. (38) by continuation using AUTO07P software,⁶⁶ and the results are presented and discussed in Sec. VI.

B. Whitham wave hierarchy

The stability analysis of the low-dimensional model (10), (23), (29), and (21) will lead to a dispersion relation equation which can be written as

$$n\tilde{I}(c - 1) + rk^2\{c\tilde{M} + n\tilde{L}(2\phi - 1) + \tilde{M}[n - 2(n + 1)\phi]\}$$

$$- ik\text{Re}\left\{c^2 - c(\tilde{F} - n + 2(n + 1)\phi) + n\tilde{G}(2\phi - 1)\right.$$

$$\left. + \tilde{F}(2(n + 1)\phi - n)\right\} + n\tilde{I}\left(\text{Fr}^{-2} + \frac{We}{\text{Re}}k^2\right)(2\phi - 1) = 0, \tag{39}$$

where ϕ is a function of the relative thickness $\tilde{\eta}_c$ of the Newtonian layer, defined in Eq. (21). The coefficients \tilde{I} , \tilde{F} , \tilde{G} , \tilde{L} , \tilde{M} , and ϕ are computed for the base state relative thickness $\tilde{\eta}_c = s^n$.

The dispersion relation (39) corresponds to a wave hierarchy situation considered by Whitham⁶⁴ and can be reset in the canonical form,^{54,55}

$$c - c_k(k) - ik\text{Re}[c - c_{d-}(k)][c - c_{d+}(k)] = 0. \quad (40)$$

Dispersion relation (40) can be split into two parts with a $\pi/2$ phase shift. Each part of the above relation corresponds to a different kind of waves. The first kind of waves from (40) is obtained by taking the limit $Re \rightarrow 0$. In this limit, the velocity field and thus the flow rate q are utterly slaved to the evolution of the film thickness h and the waves of the first kind are governed by the mass balance Eq. (10) or, equivalently, the kinematic boundary condition (3c). These kinematic waves result from the kinematic response of the free surface to a perturbation and propagate at the speed

$$c_k = \frac{n\tilde{I} + rk^2 \{n\tilde{L}(1 - 2\phi) + \tilde{M}[2(1 + n)\phi - n]\}}{n\tilde{I} + rk^2 M}. \quad (41)$$

In the limit $k \rightarrow 0$, we obtained $c_k = 1$ which in the dimensional unit corresponds to the velocity scale V as already noticed in Sec. III. We know the fact that the dependence of c_k on the wavenumber k arises from the viscous diffusion of the momentum in the direction of the flow. This viscous dispersion effect was first noted in the work of Ruyer-Quil *et al.*⁶⁷

In contrary, the second kind of waves corresponds to the limit $Re \rightarrow \infty$. These dynamic waves are the responses of the film to the variation in momentum, hydrostatic pressure, and surface tension which are induced by deformation of the free surface. These waves propagate at the speed of

$$c_{d\pm} = \frac{1}{2} (\tilde{F} - n + 2(n+1)\phi \pm \sqrt{\Delta}), \quad (42)$$

$$\text{with } \Delta = [\tilde{F} - n + 2(n+1)\phi]^2 + 4\{[n - 2(n+1)\phi]\tilde{F} + n(1 - 2\phi)\tilde{G}\} + 4n(1 - 2\phi)\tilde{I}\tilde{F}r^{-2}, \quad (43)$$

where the coefficients can be computed at $\tilde{\eta}_c = s^n$ and $\tilde{F}r^{-2}(k^2) = (\cot \theta + We k^2)/Re$. Surface tension induced the dispersion of dynamic waves. The temporal stability condition of

the base state can be written in terms of the speeds c_k and $c_{d\pm}$ for the kinematic and dynamic waves,⁶⁴

$$c_{d-} \leq c_k \leq c_{d+}. \quad (44)$$

The condition of the base state to be marginally stable is $c_{d-} = c_k$ or $c_{d+} = c_k$. In the present case, only the latter condition can be achieved. The instability threshold arises at $k = 0$ which reflects the instability of the long-wave nature and leads to

$$Fr^2 = \frac{Re}{\cot \theta} = \frac{n\tilde{I}}{(n+1)(1 - \tilde{F}) - n\tilde{G}}. \quad (45)$$

VI. RESULTS AND DISCUSSIONS

A. Linear stability results

The generalized Orr-Sommerfeld equation for the considered flow system along with the boundary conditions is solved numerically using the spectral collocation method by the help of public domain software.⁶⁶ Different prospects of instability behavior depending on various parameters, with respect to small disturbances for the considered flow system, are elaborated in this section. We have discussed the influence of the wall velocity slip on the stability features of the flow for a wide range of flow parameters, which includes the growth rate of eigenmode, neutral stability boundary, kinematic/dynamic wave behavior, and the role of the Reynolds number.

We also have deliberated the effect of the viscosity index (n) and traveling-wave solutions of the system. Eigenvalues are calculated numerically, and limiting no-slip ($\beta = 0$) results are compared with the available results for the similar flow over a rigid inclined by Ruyer-Quil *et al.*^{54,55}

In Fig. 2, we have compared the spatial growth rate and the marginal stability conditions for given fluid properties such as the flow rate, Reynolds number, and inclination angle with respect to different slip parameter β , when the threshold $\dot{\gamma}_c$, separating the shear-thinning and the Newtonian behaviors of the fluid, is varied. As expected, both the marginal (neutral) stability curve in the $Re-k_r$ plane and the spatial growth rate $-k_i$ vary significantly with the slip parameter β , which

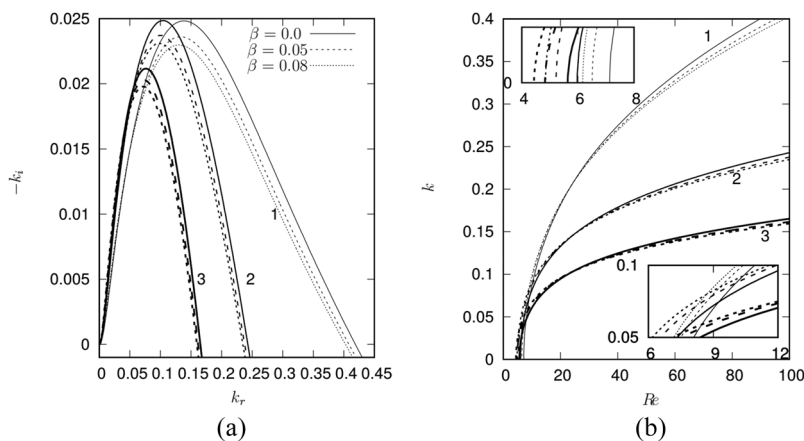


FIG. 2. Orr-Sommerfeld results (38) for xanthan gum solutions: (a) Spatial growth rate ($-k_i$) versus wavenumber (k_r) at the Reynolds number $Re = 100$ and (b) marginal stability curves in the (Re, k) plane with the cut-off wavenumber k_c . Labels of the curves refer to the parameter sets in Table I for shear-thinning xanthan gum solutions at an inclination angle $\theta = 15^\circ$. The different slip parameter values are $\beta = 0.0, 0.05,$ and 0.08 ($We \neq 0$). The curve with $\beta = 0.0$ recovers the result of Ruyer-Quil *et al.*^{54,55}

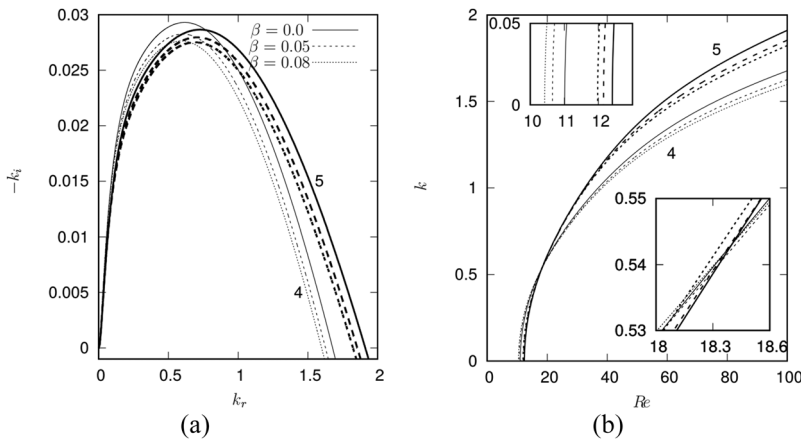


FIG. 3. Orr-Sommerfeld results (38) for cornstarch solutions: (a) Spatial growth rate ($-k_i$) as a function of the wavenumber (k_r) at $Re = 100$. (b) Marginal stability curves in the Re - k_r plane with the cut-off wavenumber k_c . Labels refer to the parameter sets in Table I for shear-thickening cornstarch solutions at an inclination angle $\theta = 15^\circ$ with different slip values $\beta = 0.0, 0.05$, and 0.08 ($We \neq 0$). The curve with $\beta = 0.0$ recovers the result of Ruyer-Quil *et al.*^{54,55}

underlines a mixed kind role on the linear instability of the flow. The results presented in Fig. 2 are obtained for the three shear-thinning fluids whose properties are detailed in Table I. Figure 2(a) presents the behavior of the spatial growth rate $-k_i$ for $Re = 100$, $\theta = 15^\circ$, and Fig. 2(b) shows the marginal/neutral stability curves, i.e., the cut-off wavenumber k_c versus the Reynolds number Re . At the considered value of Re , the wall velocity slip is trying to suppress the most excited perturbation waves by decreasing the maximum growth rate and the range of unstable wave numbers. Now, the interrogatory is whether or not this comment true for all values Re ? We have found an antithetical answer from Fig. 2(b). According to Fig. 2(b), at the onset of the instability for comparatively long waves, the slip parameter is destabilizing the flow by lowering the critical Reynolds number (Re_c). A resembling result was found by Samanta *et al.*⁵⁰ for the case of a Newtonian film flow over a slippery incline. However, after certain values of the Reynolds number and for the higher wave numbers, the wall slip is trying to stabilize the flow by diminishing the spatial growth of unstable modes.

A similar kind of result is plotted in Fig. 3 for type-4 and type-5 fluids of Table I. Qualitative behavior of the spatial

growth rate and marginal stability curves is analogous to that of the type-1, 2, and 3 fluids in Table I. However, the range of unstable wave numbers is quite high as compared to earlier cases in Fig. 2. Correspondingly, we see the existence of the bifurcation value of the Reynolds number Re_b in Figs. 2(b) and 3(b), along which the role of the wall slip parameter on the instability of the flow is changing. The values of Re_b remain between 20 and 30 for the type-1, 2, and 3 fluids and between 10 and 20 for the type-4 and type-5 fluids in Table I.

Considering the most unstable mode for each Re at the marginal condition, we have plotted the variation of phase speed for shear-thinning and shear-thickening flow in Figs. 4(a) and 4(b), respectively. Moreover, the slip parameter effect is taken into account. Quite obviously, the phase speed c of the most excited mode is decreasing for all the cases, when the viscous force is getting stronger. From earlier results, we know that the long wave instability of the system occurs at a smaller range of Re and the phase speed is comparatively high for long waves. Wall slip velocity always tends to diminish the phase speed monotonically, and this may be due to the decrease in wall shear when the slip parameter increases. The slip effect is not very promising for shear-thickening cornstarch solutions.

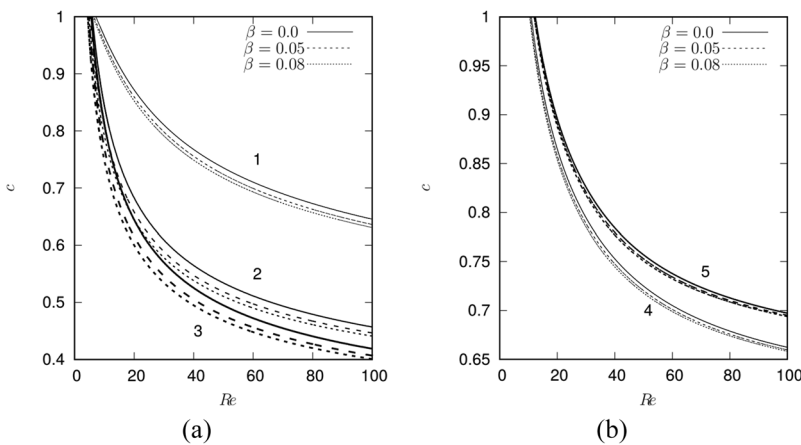


FIG. 4. Orr-Sommerfeld results (38): Phase speed c at marginal conditions versus Re plotted for (a) shear-thinning xanthan gum solutions and (b) shear-thickening cornstarch solutions at an inclination angle $\theta = 15^\circ$ with different slip values $\beta = 0.0, 0.05$, and 0.08 . Labels refer to the parameter sets in Table I.

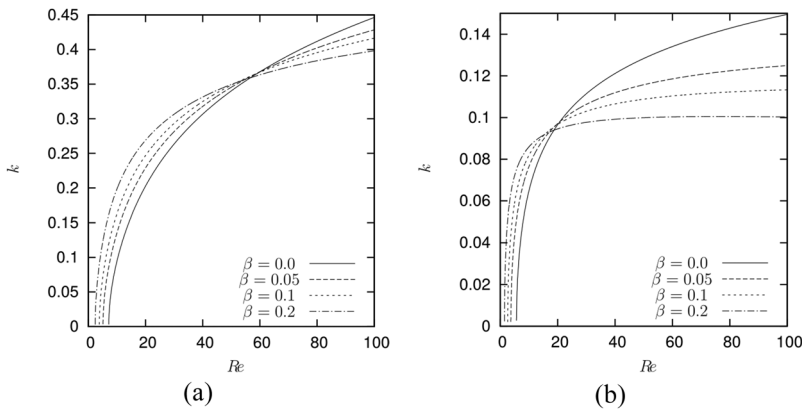


FIG. 5. The solutions to the dispersion relation of (10) and (32) show the cut-off wave number k_c versus the Reynolds number Re at an inclination angle $\theta = 15^\circ$ for (a) $n = 0.607$ and (b) $n = 0.34$ with different slip values $\beta = 0.0, 0.05, 0.1, \text{ and } 0.2$.

In Fig. 5, neutral stability boundaries are drawn for different shear-thinning fluids using the dispersion relation (10) and (32) which are derived from the averaged kinematic boundary condition and averaged momentum equation, respectively. The wall slip effect considered for two different regimes: (a) the inclined wall is a hydrophobic or a slippery type ($0 \leq \beta < 0.1$) and (b) the wall boundary is a porous kind substrate with less permeability ($0.1 \leq \beta < 0.4$).^{21,47,68-72} The qualitative impact of the wall slip on the instability is similar to the results of Fig. 5 for all values of β . It has a destabilizing influence at the onset of the free surface instability, where long waves are most excited. Very interestingly for stronger viscous forces, the moderate to shorter waves are becoming less unstable in the presence of the wall slip as compared to the no-slip case. It is also clear that as the n value decreases, the unstable region in $Re-k$ plane shrinks, indicating a stabilizing role of the effective viscosity and the relative thickness by reducing the energy transfer from the base flow to the perturbed flow.

In Fig. 6, we have presented the variations of the free surface velocity u with respect to the relative thickness s^n of the shear-thinning and shear-thickening fluids reported in Table I. The effects of n and s^n on the stability of the uniform Nusselt film solution (under Navier slip condition) are shown by capturing the variation of kinematic wave speed at the free surface. Interestingly, u_i remains less than the one whatever the values of n and s^n . Moreover, the kinematic wave speed is a monotonically increasing/decreasing function of s^n for the power-law index $n < 1/n > 1$. The smaller/larger power-law index (n) and the thinner Newtonian layer increase/decrease the speed of the kinematic wave at the free surface. Usually, a decrease in the kinematic wave speed hints the dispersive role of the streamwise second-order viscous terms, which we can refer to as a viscous dispersive effect.⁶⁷ Corresponding results for the no-slip flow (earlier work by Ruyer-Quil *et al.*^{54,55}) are available in Fig. 6(a). Comparing our slip flow results with the no-slip case, we have noticed that the kinematic wave speed in the case of the slip flow for $n < 1$ and $n > 1$ is comparatively high and low, respectively, than that of the flow with the rigid boundary (no-slip).

How the dynamic wave speeds (which compares the speed of the surface capillary-gravity waves to the fluid velocity) are changing as the function of the Froude number due to wall slip effects is shown in Fig. 7. Notably, surface tension plays a dispersive role for dynamic waves, analogous to viscosity for kinematic waves. The parameter n is varied to check the scenario for both shear-thinning and shear-thickening fluids. We have noticed that dynamic wave speed c_{d+} is overall a monotonically decreasing function of \overline{Fr}^2 for each slip and no-slip case. Moreover, the wall slip increases the dynamic wave speed because of the change in the flow rate and shear rate inside the film flow for the non-zero slip parameter. Although

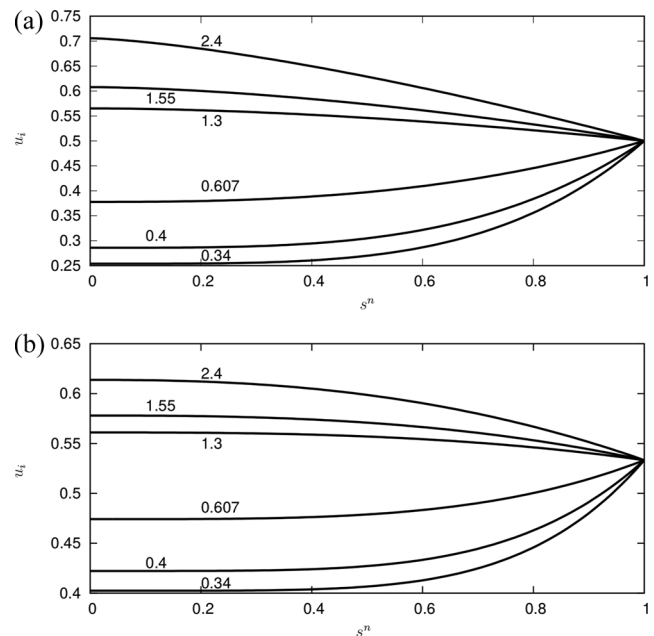


FIG. 6. Velocity at the free surface u_i as a function of the relative thickness for shear-thinning xanthan gum solutions ($n = 0.34, 0.4, \text{ and } 0.607$), and shear-thickening cornstarch solutions ($n = 1.3, 1.55, \text{ and } 2.4$) at an inclination angle $\theta = 15^\circ$ with a slip parameter value (a) $\beta = 0.0$ and (b) $\beta = 0.08$.

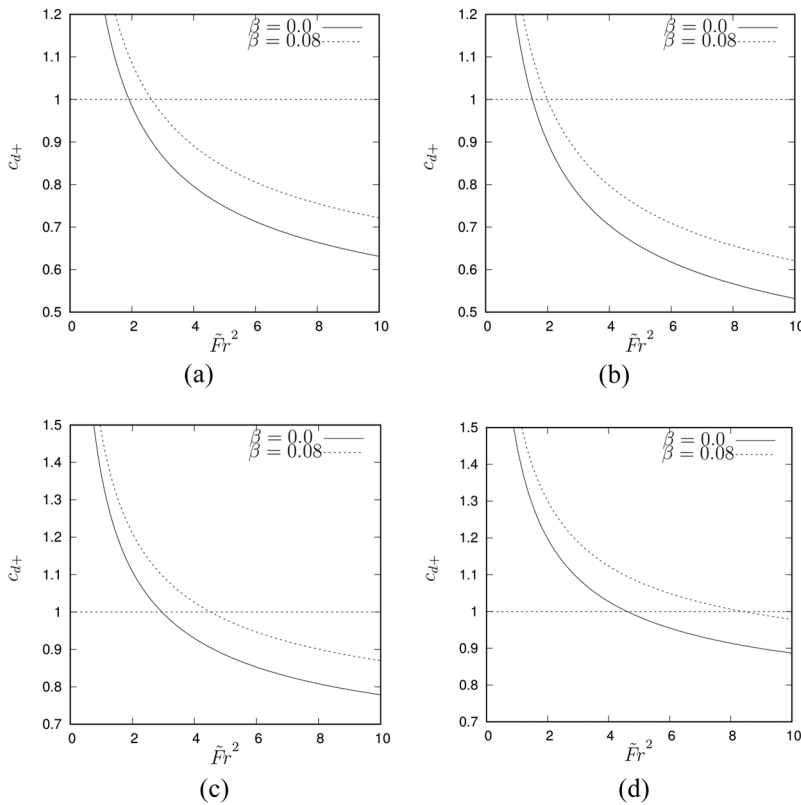


FIG. 7. Dynamic wave speed c_{d+} as a function of \tilde{Fr}^2 for shear-thinning fluids (a) $n = 0.607$ and (b) $n = 0.34$ and for shear-thickening fluids (c) $n = 1.3$ and (d) $n = 2.4$ with different slip values β . In each sub-figure, $\beta = 0.0$ curves validate the earlier no-slip case results of Ruyer-Quil *et al.*^{54,55}

the behavior of kinematic wave speed differs depending on the value of n , the qualitative nature of dynamic wave speed is unaltered for $n < 1$ and $n > 1$. However, dynamic wave speed is comparatively high for shear-thickening fluids. Overall, it may be said that a slippery substrate, therefore, contributes to destabilizing the dynamic waves but simultaneously emphasizing the viscous stabilizing dispersion of kinematic waves.⁵⁰

The movement with respect to the power-law index n of the curve $c_{d+}(Fr^2)$ governing the dynamic wave speed is illustrated in Fig. 8. Lowering the power-law index slows down the dynamic waves. Moreover, dynamic waves are basically

capillary-gravity waves advected by the free surface fluid layer which travels at half speed. The reduction in dynamic wave speed c_{d+} conversely contributes to maintaining the gap between speeds of dynamic and kinematic waves. However, such a configuration enhances the stabilizing of the decreasing kinematic wave speed by the streamwise viscous diffusion. As mentioned by Samanta *et al.*,⁵⁰ the dispersive effects of viscosity and surface tension are always tried to stabilize since they contribute to reducing the speed gap between dynamic and kinematic waves by decelerating kinematic waves and conversely accelerating dynamic waves. The downward movement of the curve $c_{d+}(Fr^2)$ is thus accompanied by a shift to

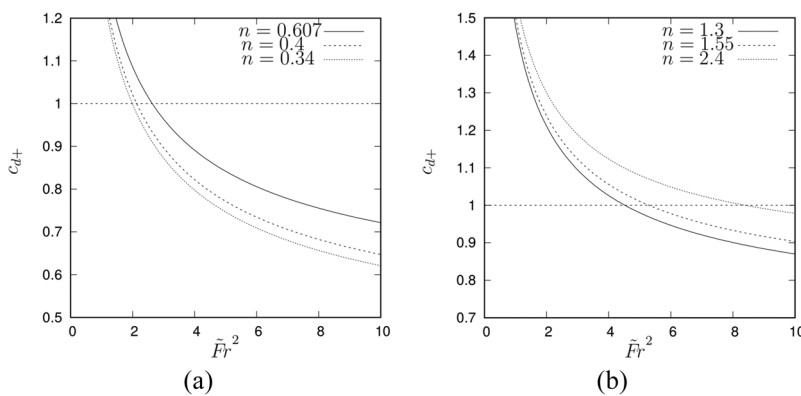


FIG. 8. Dynamic wave speed c_{d+} as a function of \tilde{Fr}^2 for (a) shear-thickening and (b) shear-thickening when the inclined wall is slippery with the slip parameter $\beta = 0.08$.

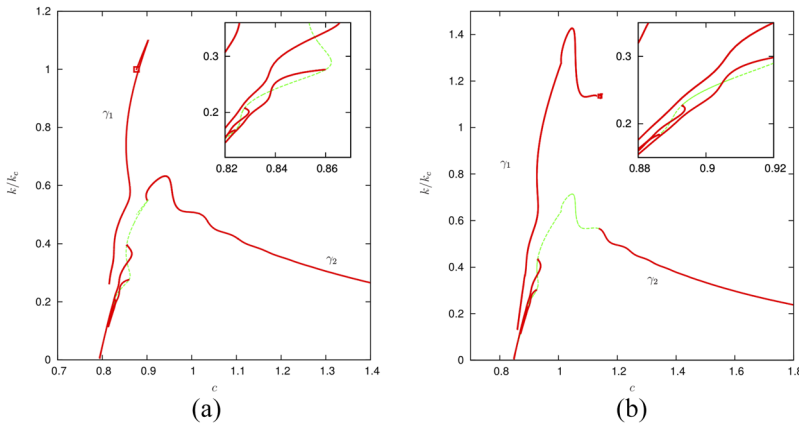


FIG. 9. Speed c of the traveling wave as a function of the wavenumber k/k_c normalized by the cut-off wavenumber k_c with the values of $Re = 20$ and $\theta = 15^\circ$ shown for (a) $\beta = 0.0$ and (b) $\beta = 0.08$. The Hopf bifurcation at k equals the cut-off wavenumber k_c that is indicated by square symbol. Dotted (dashed-dotted) lines refer to the locus of solutions made of two or four γ_1 waves. The solutions of 500 ppm shear-thinning xanthan gum solution in water (set 1 in Table I).

the left and crossing of the horizontal axis at $c_{d+} = 1$ signaling a decrease in the instability threshold. As depicted in Fig. 8(b), for shear-thickening fluids, the movement of the curve $c_{d+}(Fr^2)$ indicates that increasing n is stabilizing the system by raising the speed of dynamic waves but also stabilizing by augmenting the speed simultaneously of kinematic waves. In this case, the curves $c_{d+}(Fr^2)$ after crossing at $c_{d+} = 1$, are being displaced to the right which reflecting that the instability triggered at larger values of the critical Froude number. Note that the figures capture the variation of the curve $c_{d+}(Fr^2)$ for a slippery wall with $\beta = 0.08$. Correspondingly, no-slip case results are available in the work of Ruyer-Quil *et al.*^{54,55}

B. Bifurcation results

We have reported the bifurcation diagrams in the plane wavenumber versus speed of the traveling-wave branches in Fig. 9 considering the shear-thinning case, for the fluid properties of the three xanthan gum aqueous solutions reported in Table I over a slippery wall with $\beta = 0.08$ and a rigid wall ($\beta = 0.0$) at a moderate inclination angle $\theta = 15^\circ$ and $Re = 20$. The parameters γ_1 and γ_2 refer to the different type of waves. The first branch of slow-wave solutions arises for the most dilute solution, from the marginal stability condition $k = k_c$ through a Hopf bifurcation. Unlike the no-slip case, the number of secondary branches is found through period doubling of this first branch. We denote the principal branch of slow waves by γ_1 and the secondary branch of fast waves by γ_2 . The other secondary waves bifurcating from the principal γ_1 branch are slow. The wrinkling of the solution branches in the k - c plane and the onset of numerous secondary branches are consequences of the interaction between the typical length of the capillary ripples preceding or following the waves and the wavelength. The bifurcation diagram is quite complicated here. For the bifurcation diagram displayed in Fig. 9, traveling-wave solutions are found at larger k than the cut-off wave number k_c which corresponds to a stable Nusselt uniform film flow. Traveling waves, therefore, bifurcate sub-critically from the Nusselt solution. The wall slip influence does not change the qualitative behavior of the bifurcation diagram. In congruence with the no-slip case, the onset of sub-criticality is

here related to the large viscosity ratio between the wall and the free surface. The cut-off wavenumber is determined by the effect of the free-surface viscosity, and linear waves are efficiently damped by it. Finite amplitude disturbances may survive viscous damping by removing the Newtonian layer and thus significantly lower the viscosity at the free surface.^{54,55}

Figure 10 presents the amplitude $h_{max} - h_{min}$ versus the frequency f of the principal branch of traveling-wave solutions for a xanthan gum solution (parameter set 2 in Table I) at

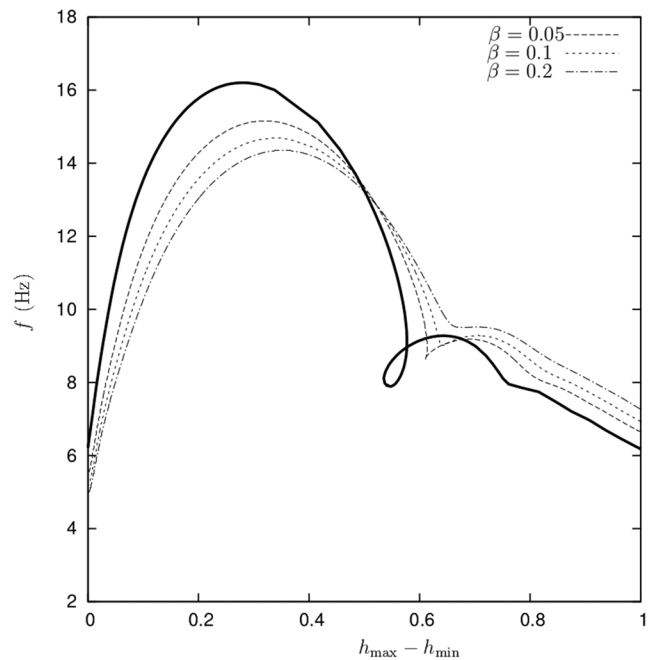


FIG. 10. Effect of the wall slip on the amplitude ($h_{max} - h_{min}$) as a function of frequency (f) at $Re = 100$. It shows the sub-critical onset of traveling waves when the frequency is varied from the cut-off frequency f_c . The inclination angle is $\theta = 15^\circ$, and the other parameters correspond to a shear-thinning xanthan gum solution (set 2 in Table I). Traveling wave solutions have been computed enforcing the open-flow condition ($\langle q \rangle = \phi_0$). The solid line refers the case of $\beta = 0$.

the slip parameter $\beta = 0.05, 0.1, \text{ and } 0.2$. The other parameters used are $Re = 100$ and $\theta = 15^\circ$. In order to enable comparisons with the wave-trains emerging from the time-dependent simulations of the spatial response of the film to a periodic excitation at frequency f , the integral constraint $\langle q \rangle = \phi_0$ has been enforced.⁷³ Traveling waves revolt at the cut-off frequency f_c from the Nusselt solution ($h_{max} - h_{min} = 0$). The presence of the slippery substrate significantly alters the dispersion of the frequency f for the amplitude $h_{max} - h_{min}$, and the influence is not uniform. The frequency f is achieving a higher/lower order value with respect to the slip parameter, depending on the critical range of amplitude $h_{max} - h_{min}$. The wall slip parameter is removing the twist from the dispersion of ($h_{max} - h_{min} = 0$), which was present in the no-slip case.

VII. CONCLUSIONS

The hydrodynamic stability of the non-Newtonian free surface flow down a slippery inclined substrate is studied. The analysis involves solving the Orr-Sommerfeld eigenvalue problem and using the long-wave theory together with the weighted-residual method. Moreover, a set of coupled evolution equations of a power-law film flow has been derived within the framework of lubrication approximation using the weighted-residual approach. A convincing agreement of the results has been found in different cases. Special attention is paid to the effects of the wall velocity slip on the instability of the considered flow system. The main objective is to predict the parameter region in which the flow is unstable and how the velocity slip can modify the stability region and parameter range.

We have derived two-dimensional models which are made of the exact mass balance equation and an averaged momentum equation and formed a set of two coupled evolution equations for the film thickness h and the flow rate q . Since the flow rate and the film thickness are, respectively, explicitly and implicitly dependent on the wall slip parameter, the solutions of model equations also rely on wall slip velocity. Consequently, the Orr-Sommerfeld solutions, namely, eigenmodes and eigenvectors, are altered by the slip effect because of the change in the base velocity. Following the argument of Ruyer-Quil *et al.*,^{54,55} we have necessarily made an adjustment at the first order of inertial terms to adequately capture the onset of the instability, whereas consistency at the second order of the viscous terms enables us to accurately account for the damping of the short waves by streamwise

viscous diffusion. However, it is not possible to consistently account for the streamwise viscous diffusion as the strain rate goes to zero. Such difficulty is avoided by introducing a bound to the effective viscosity and a Newtonian plateau at a low strain rate and dividing the flow into a Newtonian layer over a non-Newtonian bulk separated by a fake interface.

Our results show that the velocity-slip boundary condition promotes the onset of the instability and the wall slip has a destabilizing effect by lowering the critical Reynolds number. Consequently, long waves are more unstable as the slip parameter increases. However, at the moderate to large wave numbers, away from the instability threshold, a slippery substrate contributes to the weakening of instability. Thus the spatial growth rate of the system is increasing for small wave numbers with respect to the slip, followed by a bifurcation when the wave number becomes exceeding its critical value. This unexpected effect has been observed irrespective of whether the fluid is a shear-thickening or shear-thinning, and the results are consistent with that of the Newtonian film flow down a slippery wall.⁵⁰ This is the reason why the slip at the boundary at high stresses may be related to the entry flow instability instead of only the near wall instability.

We have captured the free surface velocity, dynamic wave speed, and traveling wave solution with the Navier-slip condition at the wall. The wall velocity slip enhances and reduces the free surface velocity of the disturbances for power-law indexes $n < 1$ and $n > 1$, respectively. We see a uniform decrease in dynamic wave speed as a function of the Froude number, but the wall slip ameliorates the speed of dynamic waves, which may be one of the reasons for destabilization at the onset of the instability. The higher value of the slip parameter displays a significant effect on the traveling waves and the free surface amplitude. We expect all these findings will give a clear understanding to the readers about the wall slip effects on this particular class of flow problems. Finally, results and discussions concluded that a slippery or hydrophobic surface with non-zero wall velocity can be used as a passive control option for Newtonian as well as non-Newtonian film flows.

APPENDIX: COEFFICIENTS OF THE NEWTONIAN-POWER-LAW MODEL WITH SLIP

The coefficients of (29) are presented in a fraction form $\tilde{X} = \tilde{X}_a / \tilde{X}_b$.

$$\begin{aligned} \tilde{F}_a = & 315(n + 1)^2 \left[2n^3(7n + 3) + n^2(4n + 3)(13n + 6)\beta + 3n(2n + 1)(3n + 2)(4n + 3)\beta^2 + (2n + 1)^2(3n + 2)(4n + 3)\beta^3 \right] \\ & + n(n - 1)\bar{\eta}_c^{-2+1/n} \left(105(4n + 3) \left[n^2(n(34n + 35) + 8) + 2n(n + 1)(3n + 2)(12n + 5)\beta + 6(n + 1)^2(n(6n + 7) + 2)\beta^2 \right] \right. \\ & + n(2n + 1)\bar{\eta}_c^{-2+2/n} \left[28(n - 1)(n + 1)^2(3n - 7)(4n + 3)\bar{\eta}_c - 15(n - 6)(2n + 1)(3n + 2)(4n - 3) \right] \\ & \left. + 14(4n + 3)\bar{\eta}_c^{-1+1/n} \left[3(2n + 1) \left(6n + n^2(9n(n - 4) - 4) + (n + 1)(2n + 1)(n\beta(6n - 23) + 6\beta) \right) + 10(n - 1)(n + 1)^2(3n + 2)(n + \beta + n\beta)\bar{\eta}_c \right] \right), \end{aligned} \tag{A1a}$$

$$\begin{aligned} \tilde{F}_b = & 21(n+1)(2n+1)(4n+3) \left(15(n+1) \left[2\beta^2 + n\beta(7\beta+4) + n^2(6\beta(1+\beta)+2) \right] \right. \\ & \left. + 2n(n-1)\bar{\eta}_c^{2+1/n} \left[10(3n+2)(n+\beta+n\beta) + (2n+1)(3n-7)\bar{\eta}_c^{1+1/n} \right] \right), \end{aligned} \quad (\text{A1b})$$

$$\begin{aligned} \tilde{G}_a = & 315n^3(n+1)(n(4\beta+2)+3\beta) - (n-1)\bar{\eta}_c^{2+1/n} \left(105n^2(4n+3) \left[n(10n+7) + 4(n+1)(3n+2)\beta \right] \right. \\ & + n(2n+1)\bar{\eta}_c^{2+2/n} \left[28(n-1)(n+1)^2(3n-7)(4n+3)\bar{\eta}_c - 15(n-6)(2n+1)(3n+2)(4n-3) \right] \\ & + 14(4n+3)\bar{\eta}_c^{1+1/n} \left[3(2n+1)(6\beta+n) \left[6+9\beta+n(3n^2-25n+3-3\beta(6n+5)) \right] \right] \\ & \left. + 10(n-1)(n+1)^2(3n+2)(n+\beta+n\beta)\bar{\eta}_c \right), \end{aligned} \quad (\text{A1c})$$

$$\tilde{G}_b = \frac{1}{n+1} \tilde{F}_b, \quad (\text{A1d})$$

$$\tilde{I}_a = 5(n+1)(3n+2) \left[3(n+\beta+2n\beta) + 2(n-1)\bar{\eta}_c^{2+1/n} \right], \quad (\text{A1e})$$

$$\tilde{I}_b = \frac{1}{21(2n+1)(4n+3)} \tilde{G}_b. \quad (\text{A1f})$$

REFERENCES

- ¹P. L. Kapitza and S. P. Kapitza, "Wave flow of thin layers of a viscous fluid: III. Experimental study of undulatory flow conditions," in *Collected Papers of P. L. Kapitza*, edited by D. Ter Haar (Pergamon, Oxford, 1949), pp. 690–709 [Original paper in Russian: *Zh. Ekper. Teor. Fiz.* **19**, 105–120 (1965)].
- ²S. V. Alekseenko, V. Y. Nakoryakov, and B. G. Pokusaev, *Wave Flow of Liquid Films*, 3rd ed. (Begell House, New York, 1994).
- ³N. J. Balmforth and J. J. Liu, "Roll waves in mud," *J. Fluid Mech.* **519**, 33–54 (2004).
- ⁴T. B. Benjamin, "Wave formation in laminar flow down an inclined plane," *J. Fluid Mech.* **2**, 554 (1957), corrigendum 3, 657.
- ⁵D. J. Benney, "Long waves on liquid films," *J. Math. Phys.* **45**, 150 (1966).
- ⁶H. C. Chang, "Wave evolution on a falling film," *Annu. Rev. Fluid Mech.* **26**, 103 (1994).
- ⁷H. C. Chang and E. A. Demekhin, in *Complex Wave Dynamics on Thin Films*, edited by D. Möbius and R. Miller (Elsevier, 2002).
- ⁸V. Craster and O. K. Matar, "Dynamics and stability of thin liquid films," *Rev. Mod. Phys.* **81**, 1131 (2009).
- ⁹B. S. Dandapat and A. Mukhopadhyay, "Waves on the surface of a falling power-law fluid," *Int. J. Nonlinear Mech.* **38**, 21–38 (2003).
- ¹⁰S. Kalliadasis, C. Ruyer-Quil, B. Scheid, and M. G. Velarde, *Falling Liquid Film*, Applied Mathematical Sciences, Vol. 176, 1st ed. (Springer, London, 2011).
- ¹¹J. Liu, J. D. Paul, and J. P. Gollub, "Measurements of the primary instabilities of film flows," *J. Fluid Mech.* **250**, 69 (1993).
- ¹²S. Miladinova, G. Lebonb, and E. Toshev, "Thin-film flow of a power-law liquid falling down an inclined plate," *J. Non-Newtonian Fluid Mech.* **122**, 69–78 (2004).
- ¹³C. Nakaya, "Long waves on thin fluid layer flowing down an inclined plane," *Phys. Fluids* **18**, 1407–1412 (1975).
- ¹⁴A. A. Nepomnyaschy, "Stability of wave regimes in a film flowing down on inclined plane," *Fluid Dynamics* **9**(3), 354–359 (1974).
- ¹⁵A. Oron, S. H. Davis, and S. G. Bankoff, "Long scale evolution of thin films," *Rev. Mod. Phys.* **69**, 931–980 (1997).
- ¹⁶B. Ramaswamy, S. Chippada, and S. W. Joo, "A full-scale numerical study of interfacial instabilities in thin-film flows," *J. Fluid Mech.* **325**, 163–194 (1996).
- ¹⁷C. Ruyer-Quil and P. Manneville, "Improved modeling of flows down inclined planes," *Eur. Phys. J. B* **15**, 357–369 (2000).
- ¹⁸V. Y. Shkadov, "Wave conditions in flow of thin layer of a viscous liquid under the action of gravity," *Izv. Akad. Nauk SSSR, Mekh. Zhidk. Gaza* **1**, 43 (1967).
- ¹⁹C. S. Yih, "Stability of liquid flow down an inclined plane," *Phys. Fluids* **6**, 321–334 (1963).
- ²⁰J. P. Pascal, "Linear stability of fluid flow down a porous inclined plane," *J. Phys. D: Appl. Phys.* **32**, 417–422 (1999).
- ²¹G. S. Beavers and D. D. Joseph, "Boundary conditions at a naturally permeable wall," *J. Fluid Mech.* **30**, 197–207 (1967).
- ²²M. Sadiq and R. Usha, "Thin Newtonian film flow down a porous inclined plane: Stability analysis," *Phys. Fluids* **20**, 022105 (2008).
- ²³U. Thiele, B. Goyeau, and M. G. Velarde, "Stability analysis of thin film flow along a heated porous wall," *Phys. Fluids* **21**, 014103 (2009).
- ²⁴A. Pumir, P. Manneville, and Y. Pomeau, "On solitary waves running down an inclined plane," *J. Fluid Mech.* **135**, 27–50 (1983).
- ²⁵P. A. Thompson and S. M. Troian, "A general boundary condition for liquid flow at solid surfaces," *Nature* **389**, 360 (1997).
- ²⁶Y. Zhu and S. Granick, "Rate-dependent slip of Newtonian liquid at smooth surfaces," *Phys. Rev. Lett.* **87**, 096105 (2001).
- ²⁷M. M. Denn, "Extrusion instabilities and wall slip," *Annu. Rev. Fluid Mech.* **33**, 265–287 (2001).
- ²⁸M. E. Mackay and D. J. Henson, "The effect of molecular mass and temperature on the slip of polystyrene melts at low stress levels," *J. Rheol.* **42**, 1505–1517 (1998).
- ²⁹J. M. Gersting, "Hydrodynamic stability of plane porous slip flow," *Phys. Fluids* **17**(11), 2126–2127 (1974).
- ³⁰E. Lauga and C. Cossu, "A note on the stability of slip channel flows," *Phys. Fluids* **17**, 088106 (2005).
- ³¹K. C. Sahu, A. Sameen, and R. Govindarajan, "The relative roles of divergence and velocity slip in the stability of plane channel flow," *Eur. Phys. J.: Appl. Phys.* **44**, 101–107 (2008).
- ³²X. Y. You and J. R. Zheng, "Stability of liquid-liquid stratified microchannel flow under the effects of boundary slip," *Int. J. Chem. React. Eng.* **7**, A85 (2009).
- ³³M. J. Miksis and S. H. Davis, "Slip over rough and coated surfaces," *J. Fluid Mech.* **273**, 125–139 (1994).
- ³⁴T. Min and J. Kim, "Effects of hydrophobic surface on stability and transition," *Phys. Fluids* **17**, 108106 (2005).
- ³⁵T. D. Blake, "Slip between a liquid and a solid: D. M. Tolstois (1952) theory reconsidered," *Colloids Surf.* **47**, 135–145 (1990).
- ³⁶O. I. Vinogradova, "Drainage of a thin liquid film confined between hydrophobic surface," *Langmuir* **11**, 2213–2220 (1995).
- ³⁷H. I. Andersson and O. A. Valnes, "Slip-flow boundary conditions for non-Newtonian lubrication layers," *Fluid Dyn. Res.* **24**, 211–217 (1999).
- ³⁸A. Wierschem, M. Scholle, and N. Aksel, "Vortices in film flow over strongly undulated bottom profiles at low Reynolds numbers," *Phys. Fluids* **15**, 426–435 (2003).

- ³⁹R. S. Vorono and D. V. Papavassiliou, "Review of a fluid slip over superhydrophobic surfaces and its dependence on the contact angle," *Ind. Eng. Chem. Res.* **47**, 2455–2477 (2008).
- ⁴⁰S. O. Ajadi, A. Adegoke, and A. Aziz, "Slip boundary layer flow of non-Newtonian fluid over a flat plate with convective thermal boundary condition," *Int. J. Nonlinear Sci.* **8**(3), 300–306 (2009); available at <http://internonlinearscience.org/upload/papers/20110228081012214.pdf>.
- ⁴¹S. R. Borra, "Effect of viscous dissipation on slip boundary layer flow of non-Newtonian fluid over a flat plate with convective thermal boundary condition," *Global J. Pure Appl. Sci.* **13**(7), 3403–3432 (2017); available at <https://www.ripublication.com/gjpam17/gjpamv13n7.47.pdf>.
- ⁴²E. Ellaban, J. P. Pascal, and S. J. D. D'Alessio, "Instability of a binary liquid film flowing down a slippery heated plate," *Phys. Fluids* **29**, 092105 (2017).
- ⁴³Y. J. Dai, W. X. Huang, and C. X. Xu, "Effects of Taylor-Görtler vortices on turbulent flows in a spanwise-rotating channel," *Phys. Fluids* **28**, 115104 (2016).
- ⁴⁴N. T. Chamakos, M. E. Kavousanakis, A. G. Boudouvis, and A. G. Papathanasiou, "Droplet spreading on rough surfaces: Tackling the contact line boundary condition," *Phys. Fluids* **28**, 022105 (2016).
- ⁴⁵S. Ghosh and R. Usha, "Stability of viscosity stratified flows down an incline: Role of miscibility and wall slip," *Phys. Fluids* **28**(10), 104101 (2016).
- ⁴⁶Y. M. Joshi and M. M. Denn, "Planar contraction flow with a slip boundary condition," *J. Non-Newtonian Fluid Mech.* **114**, 185–195 (2003).
- ⁴⁷M. A. A. Mahmoud, "Slip velocity effect on a non-Newtonian power-law fluid over a moving permeable surface with heat generation," *Math. Comput. Modell.* **54**, 1228–1237 (2011).
- ⁴⁸G. G. Pereira, "Effect of variable slip boundary conditions on flows of pressure driven non-Newtonian fluids," *J. Non-Newtonian Fluid Mech.* **157**, 197–206 (2009).
- ⁴⁹T. Poornima, P. Sreenivasulu, and N. Bhaskar Reddy, "Slip flow of Casson rheological fluid under variable thermal conductivity with radiation effects," *Heat Transfer Asian Res.* **44**(8), 718–737 (2015).
- ⁵⁰A. Samanta, C. Ruyer-Quil, and B. Goyeau, "A falling film down a slippery inclined plane," *J. Fluid Mech.* **684**, 353–383 (2011).
- ⁵¹J. Liu and J. P. Gollub, "Solitary wave dynamics of film flows," *Phys. Fluids* **6**, 1702–1712 (1994).
- ⁵²M. Vlachogiannis and V. Bontozoglou, "Observations of solitary wave dynamics of film flows," *J. Fluid Mech.* **435**, 191 (2001).
- ⁵³H. C. Chang, E. A. Demekhin, E. Kalaidin, and Y. Ye, "Coarsening dynamics of falling-film solitary waves," *Phys. Rev.* **54**, 1467–1477 (1996).
- ⁵⁴C. Ruyer-Quil, S. Chakraborty, and B. S. Dandapat, "Wavy regime of a power-law film flow," *J. Fluid Mech.* **692**, 220–256 (2012).
- ⁵⁵C. Ruyer-Quil, "Instabilities and modeling of falling film flows," *Fluids Mechanics* (Université Pierre et Marie Curie, Paris VI, France, 2012).
- ⁵⁶M. Amaouche, A. Djema, and L. Bourdache, "A modified Shkadov's model for thin film flow of a power law fluid over an inclined surface," *C. R. Mec.* **337**(1), 48–52 (2009).
- ⁵⁷E. D. Fernández-Nieto, P. Noble, and J. P. Vila, "Shallow water equations for non-Newtonian fluids," *J. Non-Newtonian Fluid Mech.* **165**(13–14), 712–732 (2010).
- ⁵⁸E. Brown and H. M. Jaeger, "Shear thickening in concentrated suspensions: Phenomenology, mechanisms and relations to jamming," *Rep. Prog. Phys.* **77**(4), 046602 (2014).
- ⁵⁹A. Björn, P. S. de La Monja, A. Karlsson, J. Ejlertsson, and B. H. Svensson, in *Rheological Characterization*, Biogas, edited by Dr. Sunil Kumar (IntechOpen, 2012), Chap. 3, pp. 63–76.
- ⁶⁰H. W. Bewersdorff and R. P. Singh, "Rheological and drag reduction characteristics of xanthan gum solutions," *Rheol. Acta* **27**, 617–627 (1988).
- ⁶¹A. Lindner, D. Bonn, and J. Meunier, "Viscous fingering in a shear-thinning fluid," *Phys. Fluids* **12**, 256–261 (2000).
- ⁶²G. K. Seevaratnam, Y. Suo, E. Ramé, L. M. Walker, L. M. Walker, and S. Garoff, "Dynamic wetting of shear thinning fluids," *Phys. Fluids* **19**, 012103 (2007).
- ⁶³R. G. Griskey, D. G. Nechrebecki, P. J. Notheis, and R. T. Balmer, "Rheological and pipeline flow behavior of corn starch dispersion," *J. Rheol.* **29**, 349–360 (1985).
- ⁶⁴G. B. Whitham, *Linear and Nonlinear Waves* (Wiley-Interscience, 1974).
- ⁶⁵S. Chakraborty, "Dynamics and stability of a non-Newtonian falling film," Ph.D. thesis, University of Pierre and Marie Curie, Paris 6, France, 2012.
- ⁶⁶E. J. Doedel, AUTO07P Continuation and Bifurcation Software for Ordinary Differential Equations, Montreal Concordia University, 1997.
- ⁶⁷C. Ruyer-Quil, P. Trevelyan, F. Giorgiutti-Dauphiné, C. Duprat, and S. Kalliadasis, "Modelling film flows down a fibre," *J. Fluid Mech.* **603**, 431–462 (2008).
- ⁶⁸M. Sajid, M. Awais, S. Nadeem, and T. Hayat, "The influence of slip condition on thin film flow of a fourth grade fluid by the homotopy analysis method," *Comput. Math. Appl.* **56**, 2019–2026 (2008).
- ⁶⁹L. Ren and D. Xia, "Generalized Reynolds-Orr energy equation with wall slip," *Appl. Mech. Mater.* **117–119**, 674–678 (2012).
- ⁷⁰N. Khan and T. Mahmood, "The influence of slip condition on the thin film flow of a third order fluid," *Int. J. Nonlinear Sci.* **13**(1), 105–116 (2012); available at <https://pdfs.semanticscholar.org/7c8e/36e655a6c1f7eaf8f0e27f8b1ee7308ead15.pdf>.
- ⁷¹J. Hirschhorn, M. Madsen, A. Mastroberardino, and J. I. Siddique, "Magneto-hydrodynamic boundary layer slip flow and heat transfer of power law fluid over a flat plate," *J. Appl. Fluid Mech.* **9**(1), 11–17 (2016).
- ⁷²R. Usha and Y. Anjalaiah, "Steady solution and spatial stability of gravity-driven thin-film flow: Reconstruction of an uneven slippery bottom substrate," *Acta Mech.* **227**, 1685–1709 (2016).
- ⁷³B. Scheid, C. Ruyer-Quil, S. Kalliadasis, M. G. Velarde, and R. K. Zeytounian, "Thermocapillary long waves in a liquid film flow. Part 2. Linear stability and nonlinear waves," *J. Fluid Mech.* **538**, 223–244 (2005).